UNIVERSITÀ DEGLI STUDI DI PADOVA

Dipartimento di Ingegneria Civile, Edile e Ambientale – DICEA

Corso di Laurea Magistrale in Ingegneria Civile indirizzo Idraulico

Analysis of the deposition of bedload particles

Analisi del deposito nel trasporto di fondo

Relatore: **prof. Andrea Marion**

Correlatore: prof. Simon Tait

Laureanda: **Marta Bianchini**

***Matricola*: 1079129**

Anno accademico

2014/2015

Summary

Riassunto in lingua italiana

La presente tesi si propone di indagare un aspetto finora poco esplorato del trasporto solido: il deposito dei sedimenti. Molte sono state infatti le ricerche sull' "entrainment", ovvero su quel particolare momento in cui i sedimenti, partendo da fermi, iniziano il loro moto sul fondo di un corpo d'acqua. Analogamente è stato approfondito lo spostamento dei sedimenti, con la differenziazione del loro movimento in slittamento, saltamento e rotolamento. Nessuna ricerca particolare è però mai stata sviluppata sul momento nel quale i sedimenti, dal loro stato di moto, si fermano. Quello che in particolare si vuole indagare è se esista una vera ragione per la quale il processo di deposizione avviene o se invece sia solamente un evento casuale.

I. Gli esperimenti

A tale scopo si sono utilizzati gli esperimenti effettuati nel laboratorio dell'università di Bradford nel 2009. I test originali sono dodici, ma soltanto cinque erano stati analizzati e un sesto è stato analizzato per sviluppare più dettagliatamente questa ricerca.

Nei test, tre fotocamere scattavano delle immagini ogni 0.022 s al fondo di una canaletta, permettendo di avere, alla fine dei circa 2 minuti di ogni test, 6000 immagini che mostrassero lo spostamento dei sedimenti durante il tempo di analisi. I dodici test erano stati effettuati con valori crescenti dello sforzo tangenziale e quindi della velocità di attrito.

L'analisi dei test prevedeva lo scorrimento di tutte le 6000 immagini e l'individuazione di ogni grano, visibile, in moto, distinguendo il movimento in "start", se un grano iniziava a muoversi da fermo, "move" se era già in movimento" e "stop" se si fermava.

Per l'analisi sono stati considerati soltanto i grani ai quali, durante l'analisi, fosse stato assegnato uno "stop".

II. L'analisi della deposizione

Le posizioni di tutti gli stops di uno stesso test sono state mappate all'interno dell'area analizzata, divisa poi successivamente in una griglia. Era evidente come alcune maglie della griglia fossero vuote mentre alcune fossero molto ricche di grani, facendo sembrare il

processo non casuale. Statisticamente questo è stato dimostrato con un test Chi Quadro, in cui l'ipotesi nulla era che la posizione fosse assolutamente random, e seguiva dunque una distribuzione di Poisson. Utilizzando un livello di significatività del 5% e ripetendo il test per tutti gli esperimenti e per diversi archi temporali, si nota come la distribuzione risulti a volte essere random all'inizio di un test, solitamente per i primi 20 secondi circa, e poi invece si abbia un valore del coefficiente Chi Quadro decisamente molto maggiore del valore di riferimento, indice di una decisa non casualità.

Questo andamento variabile nel tempo ha portato subito a pensare che la causa del deposito fosse la scabrezza del fondo: nel tempo alcune particelle si depositavano diventando una barriera per le successive particelle, che quindi si fermavano incidendo sulle prime.

Purtroppo però negli esperimenti di Bradford nessuna misurazione è stata effettuata per quanto riguarda la scabrezza del fondo ed era soltanto possibile indagare ed eventualmente escludere altre cause.

Inizialmente si è analizzata la posizione dei grani fine a se stessa, calcolando le distanze reciproche tra le diverse particelle e creando una distribuzione pdf di tali distanze, al fine di ottenere una "distanza caratteristica". Questa distanza d doveva essere significativa in quanto se due sedimenti avevano una distanza reciproca minore di d, allora si influenzavano a vicenda; viceversa erano indipendenti. La distanza d è stata identificata come compresa tra i 40 e i 60 mm per tutti i test, ad eccezione di quello del 22 settembre 2009, nel quale la frequenza maggiore risultava tra i 20 e i 40 mm. Di fatto però questa distanza non permetteva di trarre alcuna conclusione sulla causa della deposizione. Si è analizzata quindi anche una possibile autocorrelazione tra le distanze reciproche: si sono prese la distanze reciproche dei primi 5 stops, cronologicamente parlando, e successivamente quelle dei secondi 5 stops creando un autocorrelazione temporale tra questi primi due gruppi di stops, ottenendo un coefficiente di autocorrelazione che varia tra -1 e 1. Si è proseguita l'indagine fino all'analisi di tutti i gruppi di 5 stops, ottenendo un coefficiente di autocorrelazione medio che si aggirava intorno allo zero per ogni test. Questa analisi non ha dunque portato ad alcun risultato significativo e per questo si è dovuto esplorare qualcosa di diverso.

III. La correlazione tra deposizione e velocità

Oltre che dalle tre fotocamere, i test di Bradford sono stati monitorati da una PIV (Particle Image Velocimetry), uno strumento in grado di prendere misure di velocità nelle tre direzioni x,y e z nel tempo, generando quindi risultati in 4 dimensioni. Le velocità sono state prese nei nodi di una griglia avente maglie di 1,3 mm lungo x e 1,2 mm lungo y. La velocità è stata mediata inizialmente nel tempo, ottenendo una matrice ogni 100 immagini (2.2 secondi) ed è stato creato un contour plot, ovvero un grafico nel quale venivano riconosciute e identificate dallo stesso colore le aree soggette alla stessa velocità. Sopra tale grafico sono stati plottati anche gli stops, cercando di captarne una prima impressione visiva. Se le due grandezze fossero state correlate infatti si sarebbe dovuto vedere un gran numero di stops nelle aree a bassa o alta velocità. I grafici non mostravano però alcuna correlazione tra la posizione degli stop e la velocità.

Era necessario però anche un approccio analitico. Si è così mediata la velocità anche nello spazio, dividendo la matrice della velocità nella stessa griglia in cui erano stati divisi gli stops e calcolando una singola velocità media per ogni maglia. Essendo ora la matrice degli stop e quella della velocità della stessa dimensione era possibile il calcolo di un coefficiente di correlazione, il quale però risulta essere vicinissimo allo zero per ogni esperimento e per ogni finestra temporale.

Questo dimostra che la velocità e processo di deposizione sono tra loro indipendenti.

Benché tale risultato sia molto significativo, resta da verificare la possibile dipendenza tra la deposizione e la scabrezza del letto e sarebbe importante che in futuro fossero sviluppati nuovi esperimenti in grado di monitorare contemporaneamente nel tempo il moto dei grani e la topografia del letto.

Abstract

Bedload is defined as the components of bed particles that move in the bed layer. The motion of bed particles occurs by rolling, sliding, and sometimes, jumping (Einstein, 1950). This definition does not include the finer sediments because once disturbed, they move outside the bedlayer and go into suspension.

The question of bedload transport has been studied for over a hundred years and it is still evolving. Thanks to the literature it is now possible to know which aspects have been investigated and which have not. A lot of studies focused on the collective motion of particles with development of diffusion process or vertical mixing, while other works looked at the mechanics of the individual sediment motion: entrainment, displacement, distrainment and repose. Multiple works describe the particle entrainment: the causes, which stochastic process better describes the phenomenon and which probability distribution is followed. More recent studies usually define the different phases of particle motion, but they sometimes lack explanation on the reason "why" some of the phases happen.

It seems that most attention had been paid on the "start", but why does a particle stop? The objective of this thesis is to find out the reasons why a particle "stops". Is it just a random process, or are there any correlations between the positions in which "the stop" happens? For instance, does a change in the local flow velocity field, or the grains disposition, or the roughness of the bed affect the motion of a particle?

The study starts with the tracking of grains in one of the twelve experiments made by Tregnaghi et al. in 2009, in particular the one made on the 1st October 2009. In these experiments an area of 220 mm by 80 mm located on the centerline of a 12 m long, 0.5 m wide flume was observed with three different cameras situated above the surfaces. Two of them had a green filter and were used to measure flow field information taking frames with a frequency of 45 Hz , while the last one was used to obtain data on the particles entrainment, displacement and distrainment.

Introduction

The purpose of the present introduction is to offer a short review about the current knowledge of bedload transport.

This topic could be divided into two main aspects: the individual and the collective motion of particles.

Individual motion

The motion of individual bedload particles can be broken down into the episodic repetition of three successive phases entrainment (a), displacement (b) and distrainment (c) (Drake, 1988).

(a) ENTRAINMENT

As grains can vibrate or revolve around a vertical axis without moving their centres of mass, "entrainment" should be defined as the movement of a particle for a distance greater than 2 diametres. The particle's entrainment certainly is the better-investigated phase.

An important question was to find the initial critical condition thanks to which the motion can start. Some workers believed that the problem could be overcome by extrapolating the bedload transport curve back to the point at which transport was zero: this procedure was for example undertook by Shields in 1936 with the following formula:

$$\frac{\bar{\tau}}{(\gamma_s - \gamma_w)d} = f\left(\frac{u * d}{\upsilon}\right)$$

Where $\bar{\tau}$ is the average shear stress exerted by the fluid on the boundary at the flow stage when the particles start motion.

In 1959 Bagnold related first the particles motion with the bed shear stress and then he stated that the bedload transport was proportional to the available power of the stream, that is the rate of energy dissipation against the bed and banks of a river or stream per unit downstream length.

In 1970 Grass tackled the incipient motion starting from Shields formula: he thought that the problem lays in the definition of $\bar{\tau}$ because it is impossible to define a flow stage in which all the particles start moving all together. He reckoned that the movement takes place gradually.

Another problem in Shields' formulation is about the transport diagram resulting from the influence of turbulence, which is fully developed in a laboratory flume, but for other structures the framework of the boundary region turbulence changes and no longer shows similarities with respect to the average critical shear stress value. (Grass 1970)

Grass also developed a new theory based on the fact that every grain is potentially susceptible to a local instantaneous critical bed shear stress and using a stochastic approach this stress has a probability distribution.

After his experiment he concluded that "the instantaneous critical bed shear stress τ_c was the dominant correlating variable and both the acceleration forces (time derivative of τ_c) and the bed pressure fluctuation forces appeared to be of second importance".

The probability density function for the instantaneous shear stress was constructed from a histogram plot:

$$\bar{\tau} = \frac{\bar{\tau_c}(1 - 0.3n)}{(1 + 0.4n)}$$

Where n is a simple multiplication factor and $\bar{\tau_c} = 63.3\,\nu^{0.49} d^{0.27}$, with v=kinematic viscosity [cm^2/s] and d=mean sieve diameter of sand[cm]

In 1993 Wilcock wrote that it is necessary to relate the critical shear stress to the bed deposit composition. In particular, he distinguished between (a) unimodal and weakly bimodal sediment and (b) the ones with high degree of mixture bimodality. In the first case individual fraction begin moving at about the same flow strength: τ_c shows little variation with grain size and depends only on the mean grain size of the mixture.

In the second one finer grain sizes begin moving at measurably smaller values of bed shear stress. He found that for bimodal sediments τ_c increases with the grain size.

Hence it is possible to identify the degree of mixture bimodality at which the entrainment starts to be size dependent and the critical shear stress can be estimated using the overall grain size of the mixture, the size of each fraction, and the degree of bimodality of the mixture size distribution.

A different theory is the one of Scmeeckle et al. (2007). The study is based on the conviction that what entrains and moves sediment is the fluctuating forces, i.e. lift and drag, and not the shear stress. In fact they stated that the distribution of turbulence quantities can significantly differ between flows having identical values of average parameters, like bed shear stress.

In their experiment a force transducer was used to measure lift and drag on a test particle in three different types of bed. A Laser Doppler Velocimeter was used to measure velocity.

The experiments showed a clear coupling between the horizontal components of velocity and force. They concluded that the nominal drag is widely influenced by the instantaneous streamwise velocity and not with the instantaneous Reynold stress. That is why to predict instantaneous drag from the instantaneous velocity using the formulation of the standard drag coefficient can be considered valid.

Another approach was presented by Bottaccin and al. in 2008. The relevance of the local flow field and the movement of single grains were investigated by a series of experiments.

It was used a PIV and individual grain movements were surveyed using data from high frequency time series of images.

Clear variations in the local flow velocity field in proximity of many ‘‘start’’ and ‘‘stop’’ positions were recognized and most grain movements were associated with step changes in the time averaged longitudinal and lateral velocity.

When examining the discontinuities in both the mean and fluctuating velocity field, the majority of the significant velocity signatures were found to be located within one grain diameter of the centre of the moving grain.

Their study revisited the Grass probability distribution introducing the streamwise velocity u_f instead of the instantaneous bed shear stress. This can be done because grains entrainment u_f has a probabilistic distribution equal to the one of the Grass instantaneous shear stress τ.

The particles entrainment can take place in three different modes: rollover, which is often followed by a displacement by rolling, liftoff, often followed by a displacement by jumping, and impact ejection, followed by a displacement by rolling or sliding.

(b) DISPLACEMENT

Rolling, jumping and sliding are the three behaviors that a particle in motion can follow. According to Drake (1988) it is called "rolling" the motion less than two particle diameters between contacts with the bed. In a plan view, the particles that are subjects to rolling displacement generally trace a segmented line. Each part of the line is usually 3 or 4 diameters long. If the motion last more than two particle diameters between bed contacts its name is "jumping" or "saltating". The saltation mode of transport is confined to a layer with a maximum thickness of about 10 particle diameters, in which the particle motion is dominated by gravitational forces(Van Rijn, 1984). In a plan view the particles that are subjects to saltation displacement generally trace a straight trajectory, sometimes gently bended. Finally a particle is "sliding" if it never loses the contact with the bedlayer, usually through a flat face.

(c) DISTRAINMENT

In the experiments analyzed in the present study, it is called "stop" the absence of motion for duration equal or greater than 0.22 seconds. The complete rest of a bed particle is often dependent on the previous motion characteristics. If a particle is rolling it usually stops for gradual deceleration, if a particle is sliding

it stops for the bed roughness, by collision with some protruding bed elements, while if a particle is jumping it usually stops for a brusque impact with the bedlayer.

Collective motion

The investigation of the collective motion of particles can involve different aspects. The ones which the papers are more focused on are vertical mixing (d), bed roughness (e) and diffusion (f).

(d) VERTICAL MIXING

An important step in the studies of bedload transport was the one developed by Hassan and Church in 1994. By studying the vertical mixing of particles in a streambed, they understood that if, after a "stop", a particle is covered by other particles, it will not start again until all the particles above it will move. Furthermore the particles near the surface have more probability to move than the ones which are deeply buried. Their experiments were conducted with the introduction of tagged particles in the bed surface. Following the work of Hirano 1970, who was the first to define the "active layer" they described it as the layer of episodically mobilized material of the streambed,.. They noticed that after a single-flow peak hydrological event, the particles concentration followed with depth a negative exponential distribution, with the most of the particles near the surface and only a few deeply buried.

$$f(y) = ke^{-ky}$$

But this is not what happened after multi-peak or snowmelt events. After a few events a shift to skew-peaked and then uniform distribution was evident. After the initial dispersion, further movement of a particle depends on, among other factors, its vertical location in the bed. Deeply buried particles have less chance of being exposed and moved than others located on or close to the bed surface (Hassan and Church, 1994).

(e) BED ROUGHNESS

Back to the late 1950's the channel roughness appears to play a fundamental role in estimating bedload transport.

The problem of different particle sizes and hence of the heterogeneous bedlayer was generally dealt following two ways:

- a characteristic particle size approach
- a random field approach

At the beginning many workers, i.e. Schoklitsch and Einstein assumed that the particle size distribution of a sediment mixture may be represented by a single diameter. Traditionally, to characterize gravel-bed roughness engineers use percentiles of particle size distribution, such as 50, 65, 84, or 90%. The motivation to describe gravel-bed roughness with a single particle scale stems from the classical work of Nikuradse. (Nikora 1998)

Although, the second approach (random field) is more complete and considers all the different particle sizes.

Nikora in 1998 investigated the statistical properties of the bed elevation field Z(x, y), to create a simple model to describe bed roughness. He studies the particle sizes in longitudinal and transversal sections and found that their distributions follow, with a good approximation, a Gaussian distribution. However there is a tendency for the distribution of natural field bed profiles to be positively skewed with an average value of skewness coefficient of 0.47. Laboratory profiles show a contrary tendency of negative skewness.

The second-order structure function D(Δx, Δy) of bed elevation Z(x, y) that he defined is based on average square increment:

$$D(\Delta x, \Delta y) = \frac{1}{(N-n)(M-m)} \sum_{i=1}^{N-n} \sum_{j=1}^{M-m} \left\{ Z\left(x_i + n\delta x, y_j + m\delta y\right) - Z\left(x_i, y_j\right) \right\}^2$$

where $\Delta x = n\delta x$, $\Delta y = m\delta y$, δx and δy are the sampling intervals and N and M are the total numbers of measuring points of bed elevations in directions x and y , respectively.

A typical structure function of bed elevation has a common property which is that in most cases it consist of two main regions. At small spatial lags, structure functions behave like power functions $D(\Delta x) \propto \Delta X^{2Hx}$ and $D(\Delta y) \propto \Delta y^{2Hy}$(scaling region), while at sufficiently large lags they become constant (saturation region).(Nikora 1998)

The third, vertical scale ΔZ_o can be obtained from the saturation region as

$$\Delta Z_0 = \sqrt{D(\Delta x = \infty)/2} = \sqrt{D(\Delta y = \infty)/2} = \sigma_z$$

where σ_z is the standard deviation of bed elevation.

This means that, on average, the standard deviation of bed elevations is less than half the horizontal roughness scales.

From his study Nikora also found that if "a" is the major axis of a sediment, "b" the intermediate one and "c" the shortest, "a" will arrange transverse to the flow direction, "b" in the flow direction and "c" orthogonal to the flow direction.

(f) DIFFUSION

A very important study for particles diffusion is the one carried out by Nikora et al. (2002). For every type of displacement modes his model explains that particle motion can be divided into three different temporal and spatial scales with different diffusion regimes. Following his definitions it is possible to distinguish: (1) the local range, corresponding to ballistic particle trajectories between two successive collisions with the static bed particles, (2) the intermediate range (normal or anomalous diffusion), corresponding to particle trajectories between two successive periods of rest. These trajectories consist of many local trajectories and may include tens or hundreds of collisions with the

bed, and (3) the global range (subdiffusion) of scales corresponds to particle trajectories consisting of many intermediate trajectories, just as intermediate trajectories consist of many local trajectories.

The model presents the q^{th} central moments of the particle coordinates as a function of eight variables, $\overline{X'^q}, \overline{Y'^q} = f_q[u*, g, d, D, v, t, \rho, (\rho_s - \rho)]$ where u* is the shear velocity; g is gravity acceleration; d is diameter of a travelling particle; D is a prevailing diameter of static bed particles; v is fluid viscosity; ρ and ρ_s are densities of water and solid particles, respectively; and t is the particle travelling time including rest periods. This yields, for the case of the second moment, to $\overline{X'^2}, \overline{Y'^2} = f_2[u*, g, d, D, v, t, \rho, (\rho_s - \rho)]$, and following the Buckingham it is possible to pass from 8 dimensional quantities to 5 adimensional groups using 3 fundamental quantities:

$$\frac{\overline{X'^2}}{d^2}, \frac{\overline{Y'^2}}{d^2} = f_{2a}\left[\frac{u_*^2}{gd}, \frac{d}{D}, \frac{u_* d}{v}, \frac{t u_*}{d}, \frac{\rho}{(\rho_s - \rho)}\right]$$

Making some simplifying hypothesis is it possible to obtain:

$$\frac{\overline{X'^2}}{d^2}, \frac{\overline{Y'^2}}{d^2} = \left(\frac{t u_*}{d}\right)^{2\gamma_x, 2\gamma_y} f_{2b}\left[\frac{\rho u_*^2}{(\rho_s - \rho) g d}\right]$$

where the exponents γ_x and γ_y needs to be defined from experiments.

It is reasonable to think that small particles should have more intensive diffusion compared with larger ones, that's why in general, they may depend on the relative particle size d/D and the mode of particle motion.

Nikora's experiments showed that for large particles the diffusion is likely isotropic, that is $\gamma_x \approx \gamma_y$, while for the case of small particles it may result anisotropic as $\gamma_x < \gamma_y$.

1 The experiments

1.1Experimental apparatus

The data used to develop the present work is taken from experiments carried out from July to October 2009 in the Hydraulics Laboratory of the University of Bradford.

Figure 1.1: Laboratory flume of University of Bradford (from Guarin 2010)

A laboratory flume 12 m long and 0.5 m wide was used. The first 1.5 m of the flume was covered with gravel that guaranteed to have stable boundary conditions for all the experiments. The other part of the flume bed was filled with loose natural river gravel with a

percentiles of particle size distribution d_{50}=5 mm, a density ρ_s=2650 kg/m^3 and a size standard deviation σ=1.3. This was made in order to avoid to have any bed forms and to guarantee a uniform and well-mixed bed.

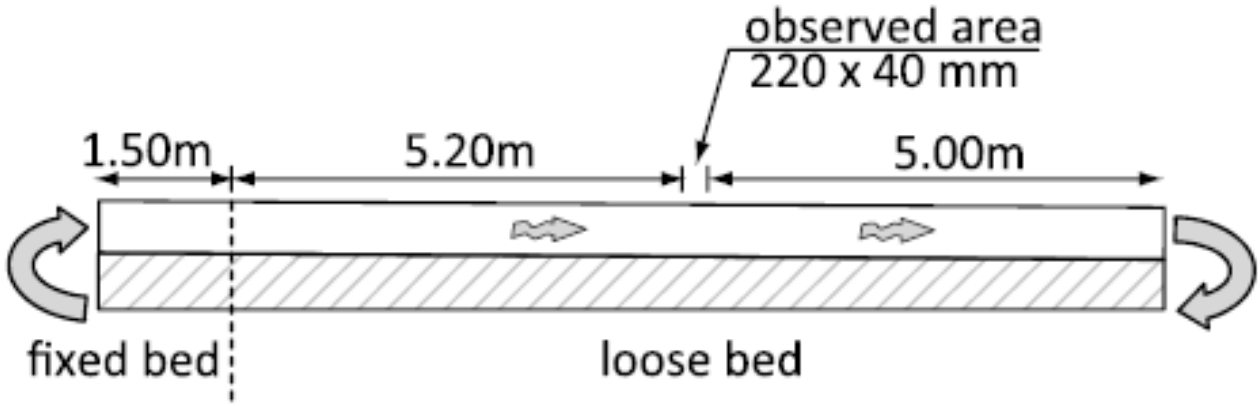

Figure 1.2: Longitudinal section of the flume (from Tregnaghi et al. 2012)

The water level was kept constant and equal to h=100 mm for all the twelve tests.

The flume slope was gradually increased during the tests sequence. A constant water discharge was induced to have steady and uniform hydraulic conditions.

For all the observations and measurements it was analysed a rectangular area situated at 6.70 m from the inlet. This area was 220 mm long and 40 mm wide and it was located on the centreline of the flume.

The size of the area was chosen to collect measurements of the velocity field in an appropriate spatial scale and to observe an adequate number of grains for each test. This allowed to achieve significant statistical data.

It was created a laser sheet with uniform intensity, located at about 10 mm from the bed surface to avoid any interferences with the bed movements and to reduce the light reflected by the bed.

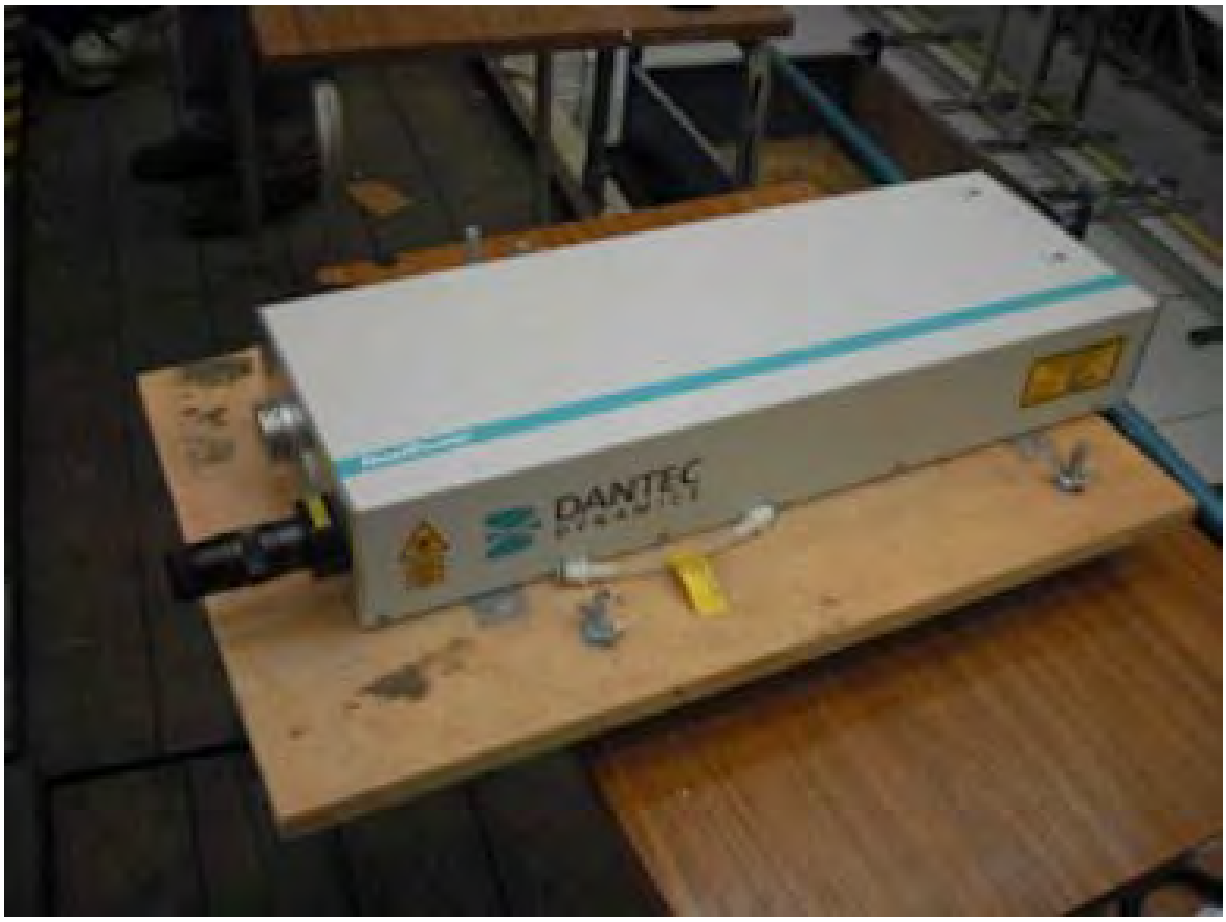

Figure 1.3: DantecDynamics experimental laser (from Guarin 2010)

A floating glass sheet was located at the same level of the water surface to avoid image distortion due to the water fluctuations.

The presence of the glass sheet could though cause the presence of bubbles in the intersection between the free water surface and the edge of the glass. The bubbles worsened the quality of the images but it was possible to reduce the interference using a baffle plate. This was situated upstream of the viewing plate and permitted a more gentle transition.

Figure 1.4: Investigation area and the downstream baffle plate (from Guarin 2010)

At the end of each experiment, sediments that reached the flume outlet were collected and reallocated.

This operation was made to ensure the same grains arrangement for all the experiments.

1.2 Instrumentation and image acquisition

The flume was equipped with a measurement system that allowed the simultaneous collection of grains entrainment and flow velocity in a near-bed plane section.

The observation area was monitored by three cameras located vertically 6.7 m from the inlet and 1.85 m from the bed surface.

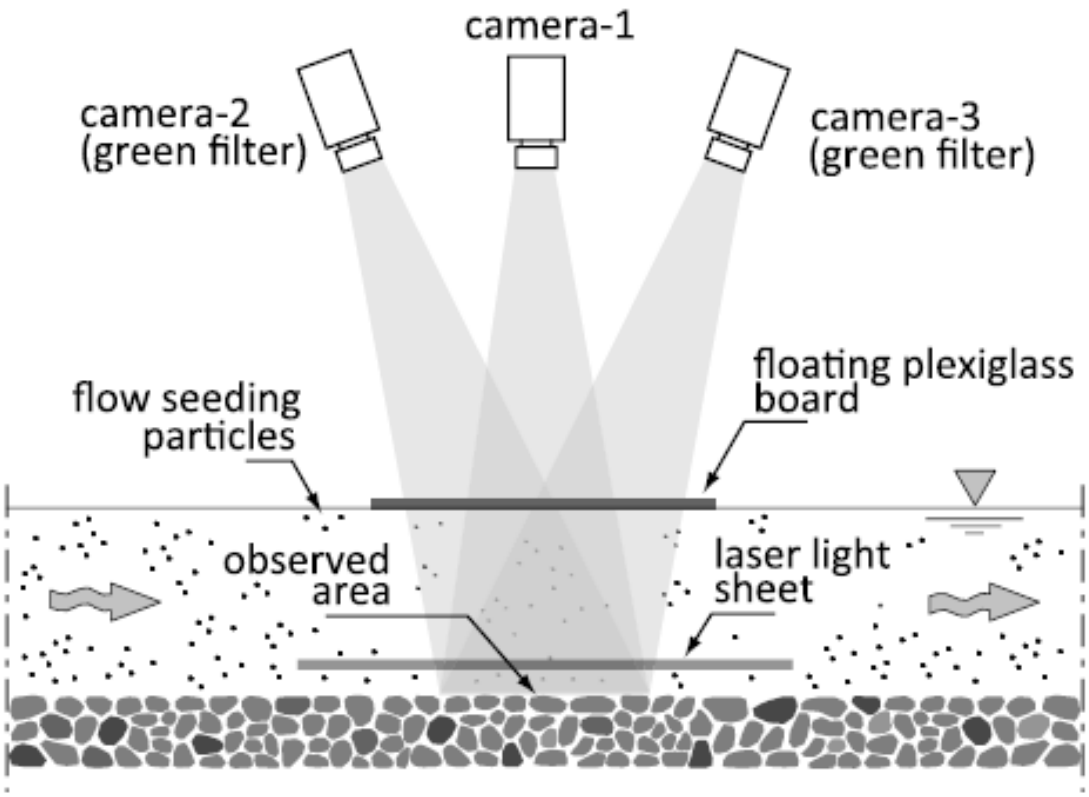

Figure 1.5: Sketch of the experimental equipment for image acquisition (from Tregnaghi and al. 2012)

The camera 1 used a white strobe light to achieve grains transport information, such as entrainment, displacement and deposition data. The camera faced the bed surface and captured an image of the bed at the starting time of the second of the paired flow images. The other cameras had a green filter and were used to obtain information about the flow field. Cameras 2 and 3 took image pairs with a time steps Δt=1 ms between images, with a frequency f=45 Hz.

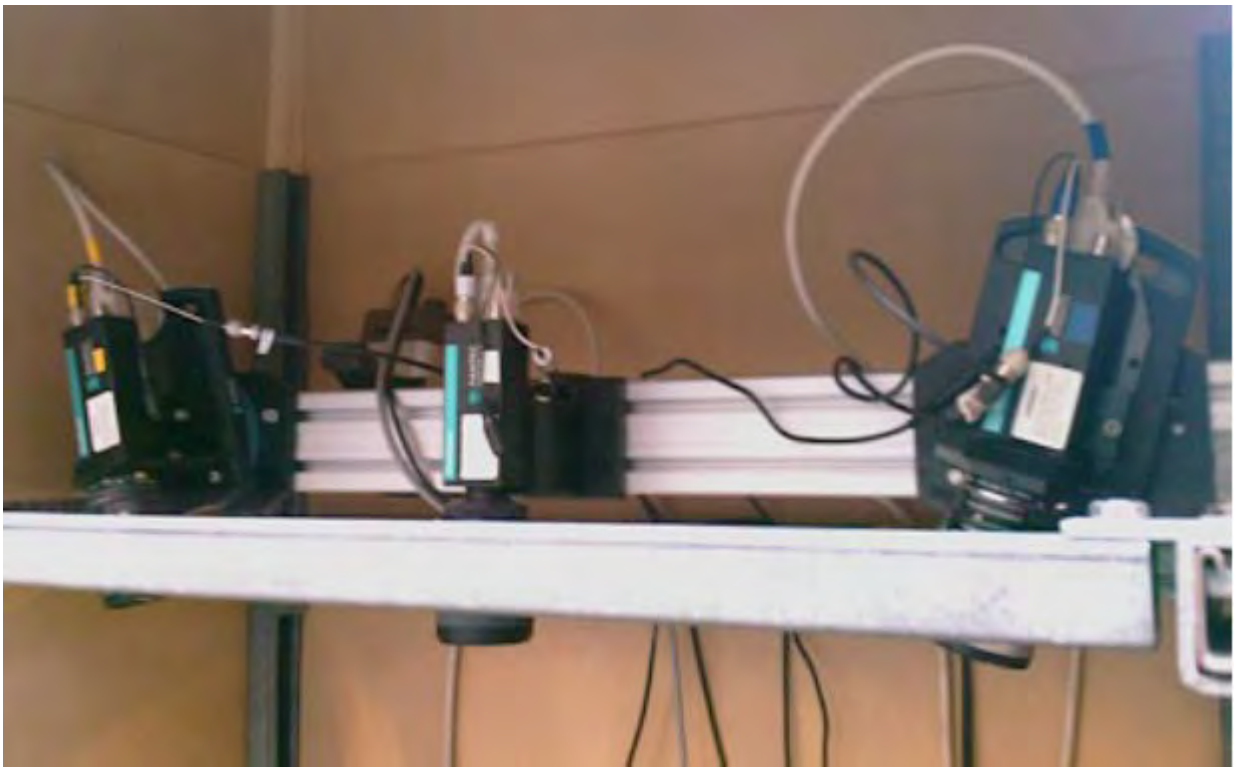

Figure 1.6: DantecDynamics experimental cameras (from Guarin 2010)

The selected area was split into smaller investigation areas, 4.3x4.3 mm^2, that is close to the size of a single grain, with an overlap of 75% between each area.

Therefore, velocities of the fluid were known on a 1.07 mm square mesh grid, with N=35x185 = 6475 nodes, located about 8-10 mm above the sediment deposit.

This allowed the collection of measurement of the near bed velocity.

The experiments used a PIV (Particle Image Velocimetry) system. This technique constitutes of a non-intrusive laser optical measurement that gives the whole velocity fields by taking two images shortly after each other and calculating the distance individual particles travelled within this time.

To obtain data from the PIV and measure the spatial flow velocity pattern, the fluid was seeded with tracer particles. These particles were spherical, made of polystyrene, with an average diameter d_{tp}=200 µm and with a density ρ_{tp}=995 kg/m^3.

Because of their low density and inertia, they were expected to follow the flow field. The laser light created a planar cross section of illuminated flow. When a tracer particle intersected the light sheet, an image was built.

1.2.1 Particle Image Velocimetry PIV

The PIV is a not intrusive optical laser measurement technique to analyse flow and turbulence. The instrument generates instantaneous measures of the velocity flow field in a cross section with high accuracy. The technique units particles into groups and finds the more probable motion. A PIV includes

- a camera
- a high power laser
- an optical instrument
- a synchronizer

Because of PIV is not intrusive, velocity measures are indirect.

It is possible to measure simultaneously the velocity flow field in a plane section and the high speed data processing allows frames generation.

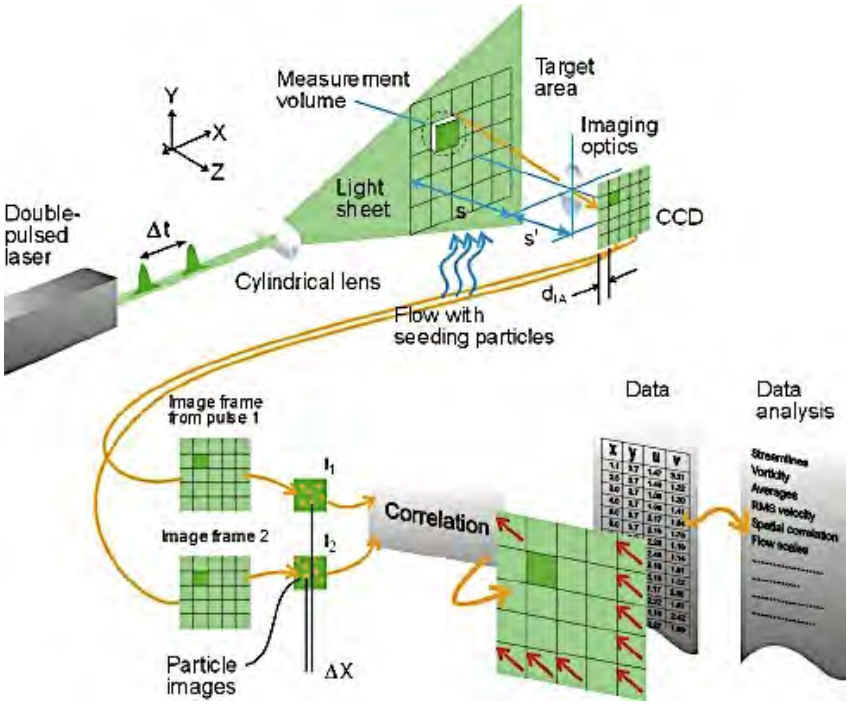

Figure 1.7: Scheme of the PIV system: measurement and processing

Sometime particles do not follow the fluid motion because of their higher density. It would be optimal to find particles having the same density of fluid, but if it is not possible everything can be made more homogeneous raising or lowering temperature.

In the present experiment the tracer particles were chosen specifically to be able to follow the fluid motion. Furthermore particles must not alter the fluid or interact with each other.

Particles typical diameter is from 10 to 100 μm:

- small enough to have a quick reaction to the motion and accurately follow the flow
- big enough to spread a significant amount of incident laser light.

Two laser light expositions above the fluid were necessary for the analysis. At the beginning cameras were not able to capture multiple frames at a high speed. Hence both the expositions were taken on the same image that was adopt to characterize the fluid using an autocorrelation process. Nevertheless the fluid direction was hard to define because it was not clear which spot particles were from the first exposition and one from the second one.

Now better cameras can take two frames at a high speed and a more accurate cross correlation process is possible because each exposition is isolated to its own frame.

Lasers emit monochromatic light with high energy density that can be wrapped together with the light sheet to enlighten and record the tracer particles without chromatic anomaly.

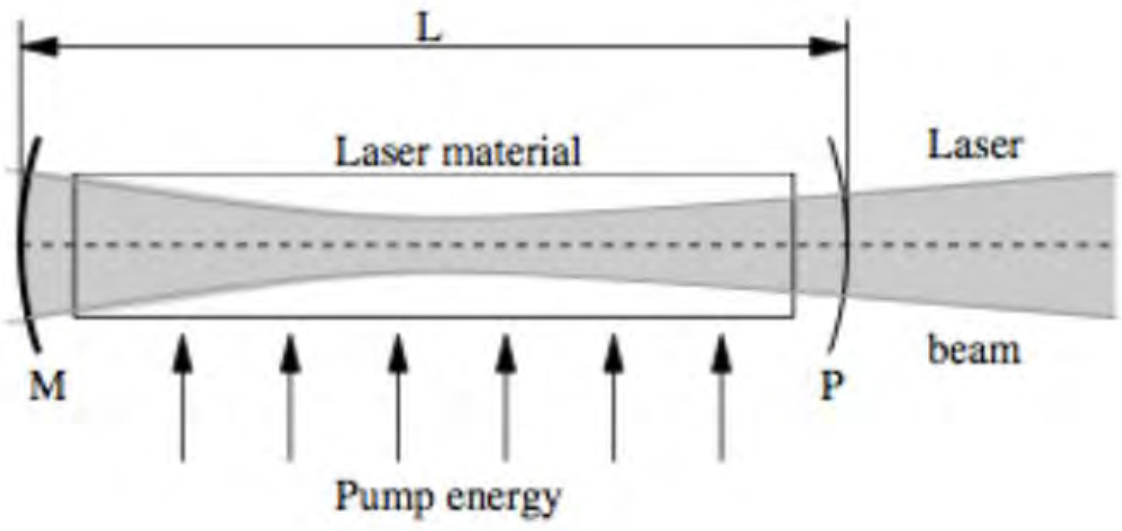

Figure 8: Schematic diagram of a laser from (Guarin 2010)

1.3 Experimental tests

Twelve tests were carried out using different slope, but maintaining the same water level. The experiments were carried out with a progressive increase of the shear stress value.

Each test was about 3 hours long but velocity and grain movement measurements were taken simultaneously for roughly 10 minutes.

Table 1.1 reports the hydrodynamic values which characterized each test.

Table 1.1: Experimental Parameters (from Tregnaghi and al. 2012)

Test	Date	S(%)	Q(l/s)	U(m/s)	$R_e(\cdot 10^5)$	u_s(m/s)	τ*0	Q(g/s)
1	06/08/2009	0,55	40,50	0,88	2,81	0,067	0,057	-
2	21/08/2009	0,57	42,60	0,93	2,93	0,069	0,059	-
3	24/08/2009	0,59	43,30	0,94	2,98	0,070	0,061	-
4	28/08/2009	0,62	43,80	0,95	3,02	0,071	0,064	-
5	02/09/2009	0,65	44,80	0,97	3,10	0,074	0,068	3,10
6	04/09/2009	0,69	45,60	0,99	3,16	0,076	0,072	-
7	09/09/2009	0,72	46,40	1,01	3,22	0,077	0,074	-
8	17/09/2009	0,75	47,20	1,03	3,28	0,079	0,077	-
9	22/09/2009	0,77	48,10	1,05	3,34	0,080	0,080	3,40
10	23/09/2009	0,8	49,00	1,07	3,40	0,081	0,083	-
11	29/09/2009	0,83	49,80	1,08	3,45	0,083	0,086	4,00
12	01/10/2009	0,86	50,90	1,11	3,53	0,085	0,090	-

The parameters are:

- S(%) : slope of the flume
- Q(l/s) : water discharge
- U(m/s) : depth average flow velocity
- $R_e(\cdot 10^5) = 4R_HU/v$: Reynolds number, where R_H is the hydraulic radius and v the kinematic viscosity
- $u_s(m/s) = (gR_HS)^{0.5}$: shear velocity, where g is the acceleration due to gravity

- $\tau_0^* = \tau_0/[g(\rho_s-\rho)d_{50}]$: Shield parameter, where τ_0 is the boundary shear stress and ρ_s and ρ are the densities of sediments and water respectively
- $Q_s(g/s)$: sediment discharge

Flow velocity distribution and grains movement could be determined in a system moving from a $\tau_0^* = 0.057$ to a $\tau_0^* = 0.090$. The aim was to move away from the threshold of motion to conditions of fully developed transport.

1.4 Grains motion

To obtain sediment transport data from the tests it was used the software GSLAB (Bottacin, Busolin et al. 2008).

An example of the frames captured by the three different cameras is visible in figures 1.7, 1.8 and 1.9.

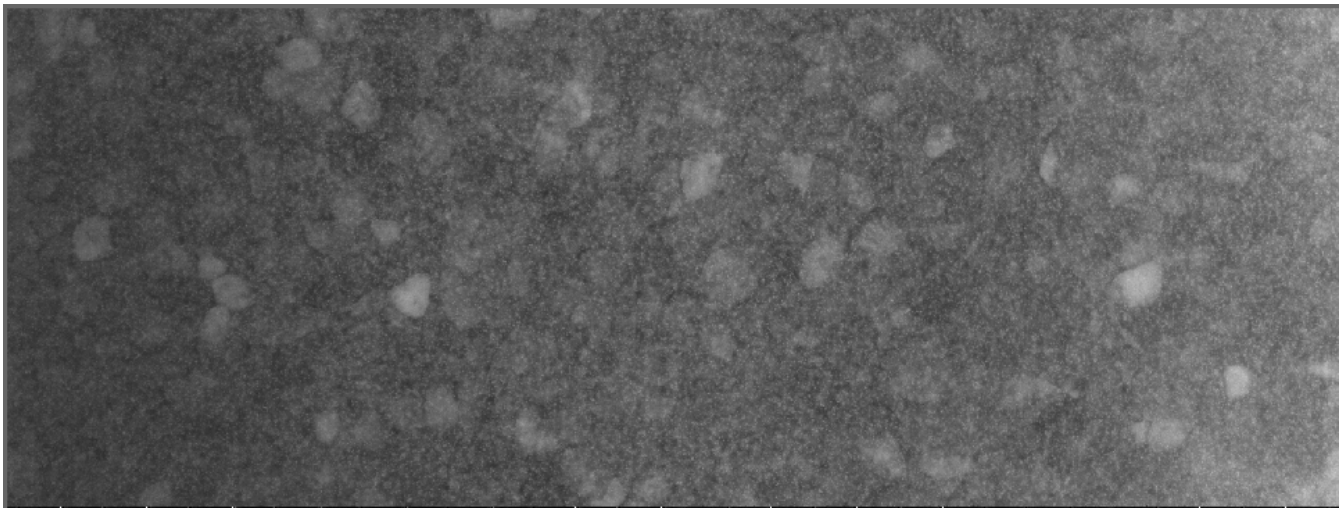

Figure 1.9: Camera 1

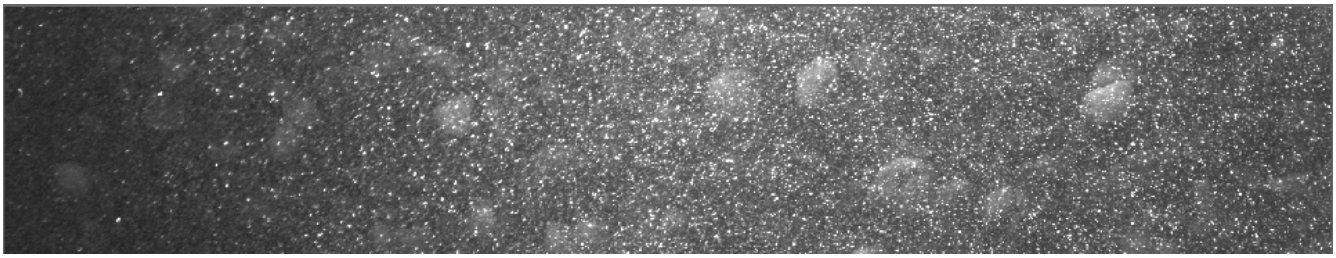

Figure 1.10: Camera 2

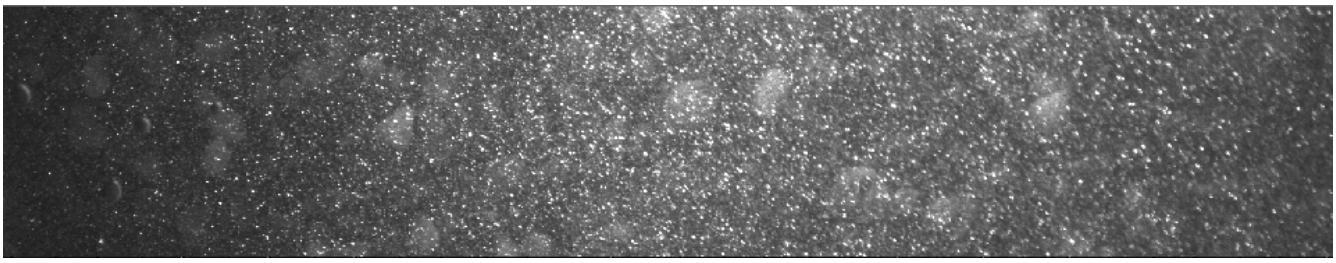

Figure 1.11: Camera 3

It is possible to observe that the cameras did not cover the same area. The frames taken by camera 1 are exactly of the same size of the investigated area, while frames captured by cameras 2 and 3 are longer and thinner but anyway useful to compare with the ones taken by camera 1.

It was possible to observe the images using the green map view option (figure 1.10).

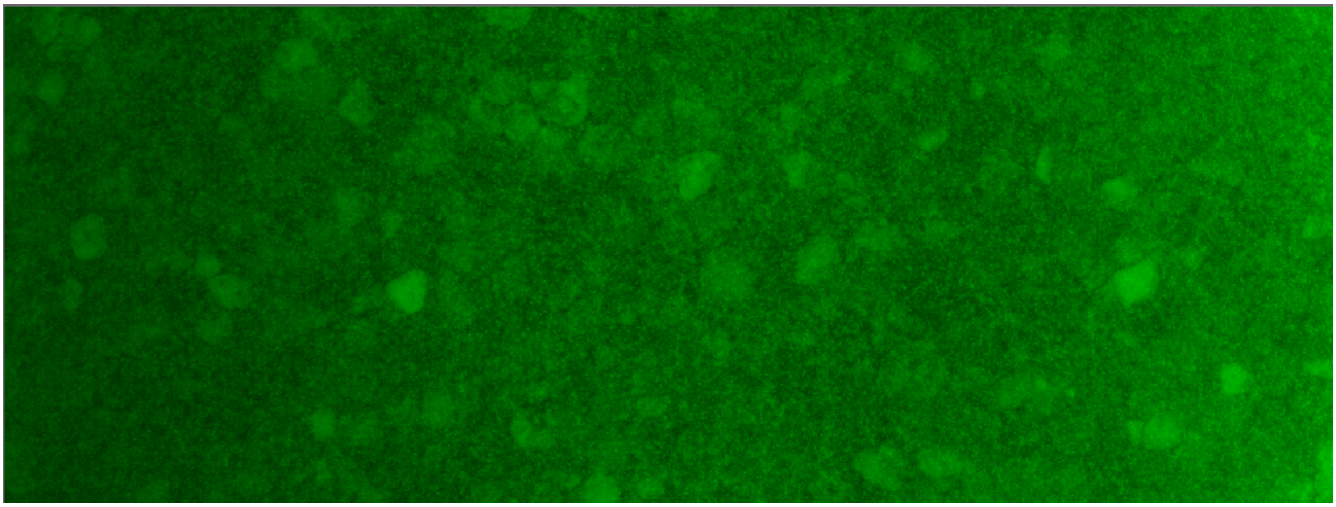

Figure 1.12: Camera 1 with green map

1.4.1 Grain Displacements

Each image describes the instantaneous arrangement of the bed sediment. The positions taken by each single particle during its displacement were divided as follow:

(1) START : if the grain is being entrained

(2) MOVE : if the grain is moving on the bed surface

(3) STOP : if the grain is deposited on the bed to rest

In general the displacement is a positional change undergone by any grain.

As already mentioned in the Introduction, a grain movement can occur by rolling, sliding or saltation. In the experiment most of grains displacement took place by saltation, sometimes by rolling and infrequently by sliding.

The grain displacements were catalogued as follow:

(1) START : if a grain started its motion inside and stopped outside the investigated area

(2) MOVE : if both entrainment and distrainment occurred outside the selected area

(3) STOP : if the sediment entrainment happened outside the area and the distrainment happened into the investigated area

(4) START-STOP: if both the grain start and stop positions are located into the investigated area

To clarify the description, Figure 1.11 represents the four different types of displacements.

In case of displacements, the distance covered was estimated while the grain was in motion and these movements were further classified based on the distance covered by the grain.

The grains, which displacements length was shorter than the particle's diameter, were all catalogued into the group "shake".

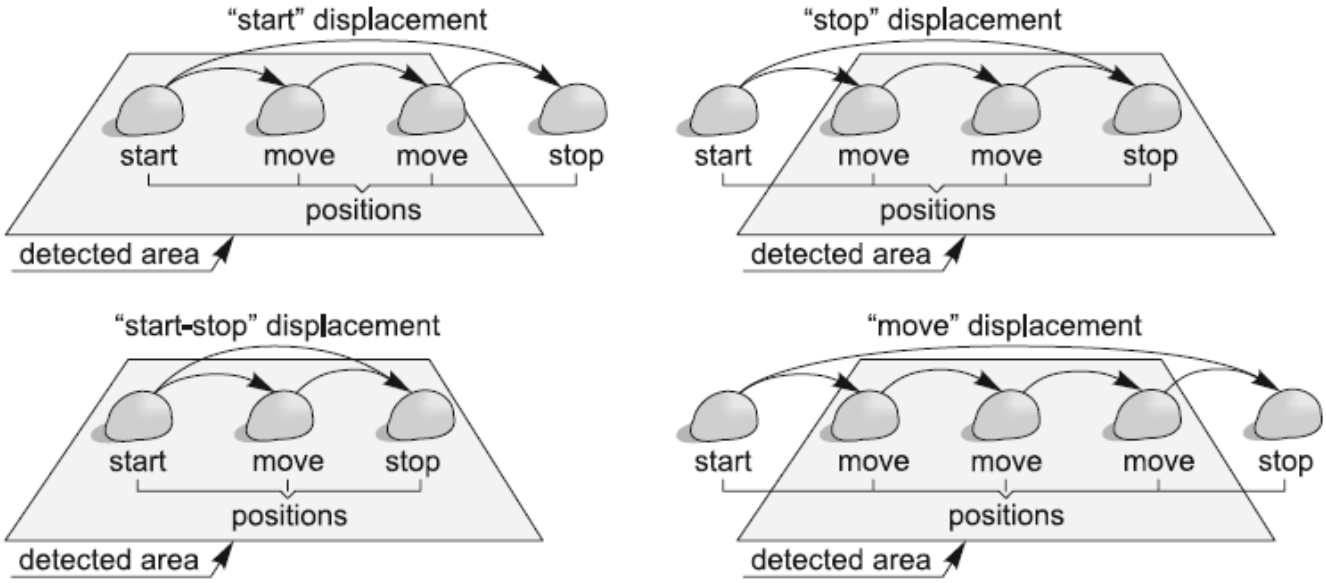

Figure 1.13: Displacement types

This type of displacement corresponds to sudden, small changes of position; oscillations of one grain around its equilibrium position were neglected. ''Shake'' movements indicate that the grain is rather ''unstable'' and the probability that is going to be entrained is very high.
The frames sequence was manually analysed. The total area was zoomed into smaller parts with a suitable scale to better recognize the particles movements.
By comparing an image with the previous and/or with the subsequent one, it was possible to observe the single grain movements over the bed surface.
When a movement was notice the procedure to adopt was the following one:

a) Identify the grain centre of gravity (figure 1.12)

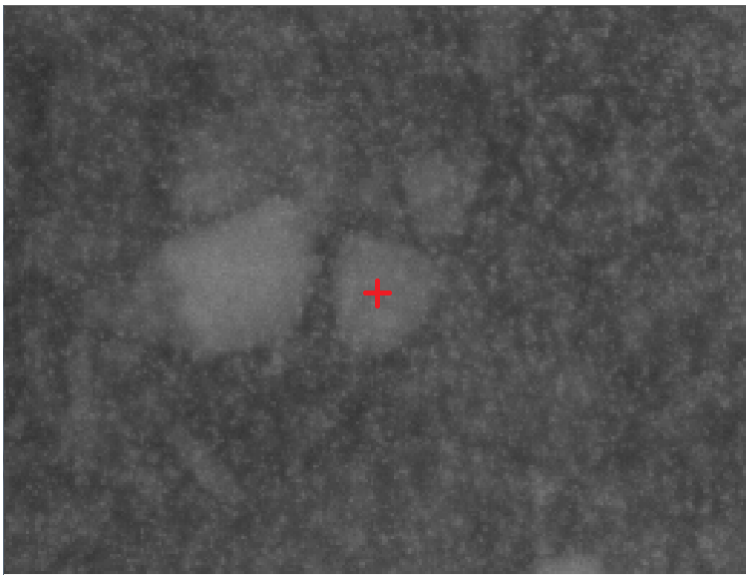

Figure 1.14: barycentre identification

b) Outline the particles (figure 1.13): it was important to detect the particle's boundary with accuracy because then a bounding box would be created around the particles and the barycentre position would be updated. GSLAB stored the x and y coordinates of the centre of gravity and of all the bounding box corners.

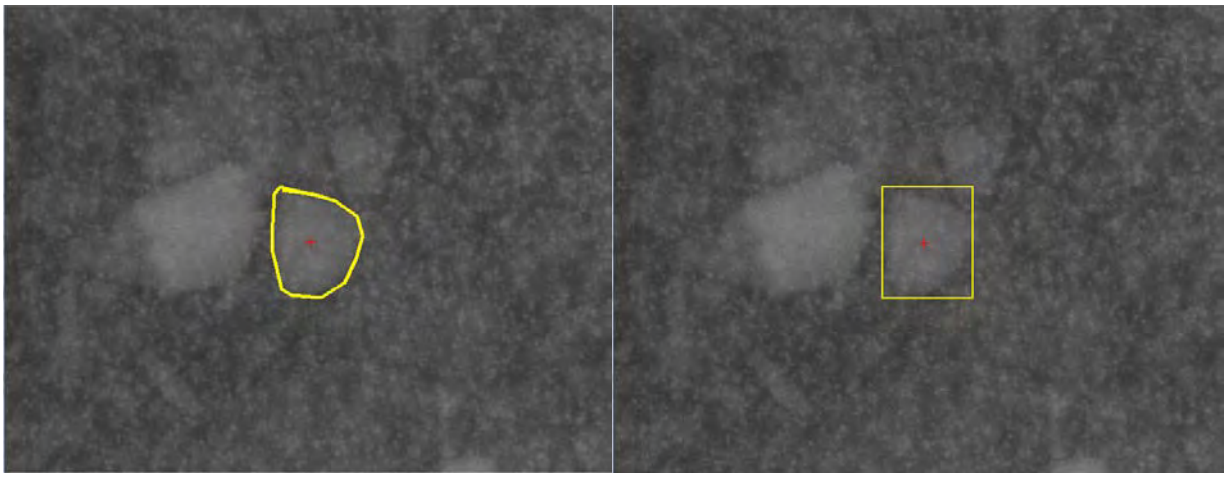

Figure 1.15: Creation of the bounding box

c) Identify the type of position taken by the particle: GSLAB makes possible to choose among the three different motions start, move and stop. It was also possible to point out if a grain was triggered into motion due to the collision with another moving grain by using the window "moved by" (figure 1.14).

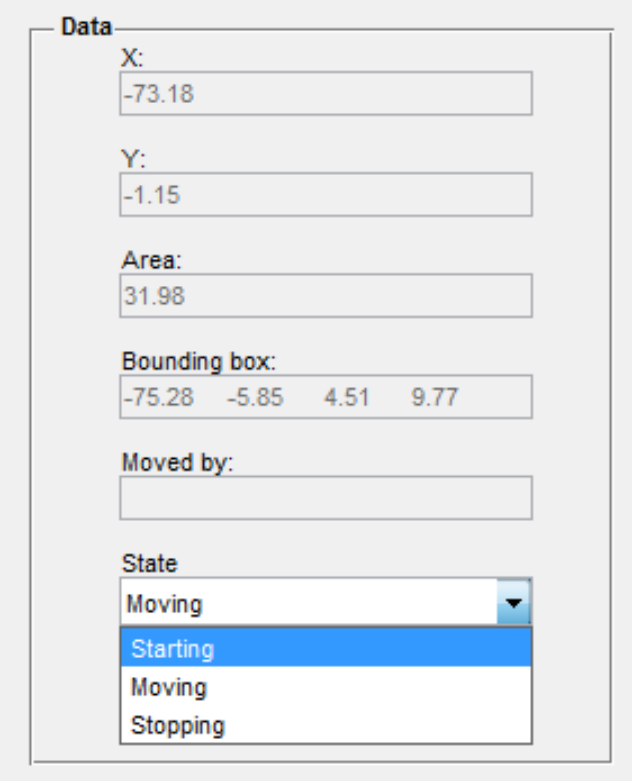

Figure 1.16: Motion types choice

d) Assign the code number (figure 1.15): each identified particle was given a number to recognize it in the following frames.

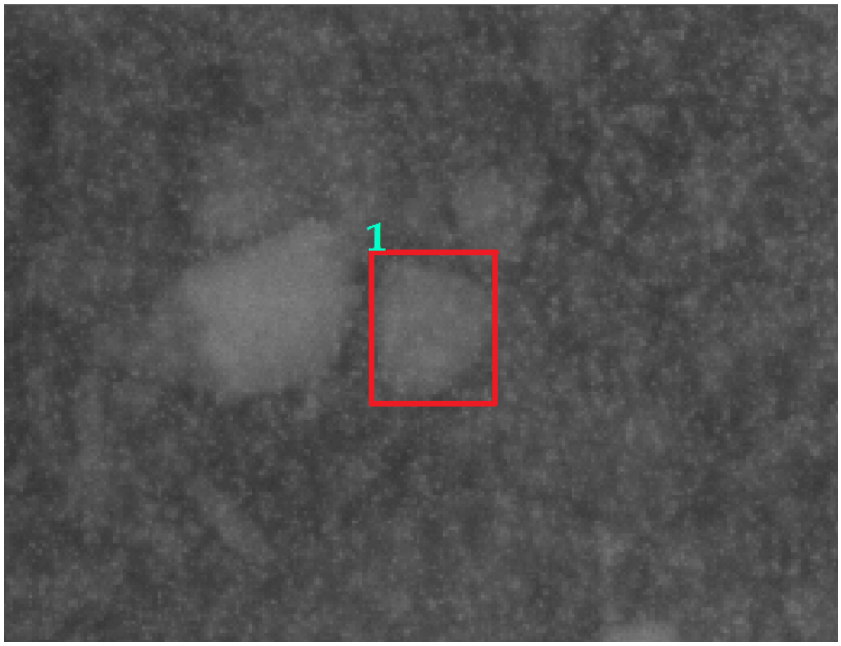

Figure 1.17: Code number assignment

Table 1.2: Code number assignment

Test	Date
1	06/08/2009
2	21/08/2009
3	24/08/2009
4	28/08/2009
5	02/09/2009
6	04/09/2009
7	09/09/2009
8	17/09/2009
9	22/09/2009
10	23/09/2009
11	29/09/2009
12	01/10/2009

Each test collected about 6000 frames with a time step:

$$\Delta t = \frac{1}{f} = \frac{1}{45Hz} = 0.022\ s$$

between two consecutive images.

Due to the great efforts spent in manually analyzing the videos, only six out of the twelve tests have been analyzed so far (table 1.2).

In particular the present work starts with the study of the test made on the 1ST October 2009, the one with the highest shear stress.

1.4.2 Examples of motion

To better understand how the different types of motion were recognised, this paragraph shows an example for each one.

It is possible to define "START" the entrainment of a particle, which was resting in the previous frame (figure 1.16).

As explained before, the entrainment of a particle can occur also because of the impact with another grain which is moving. In this case the start is defined as a "start moved by".

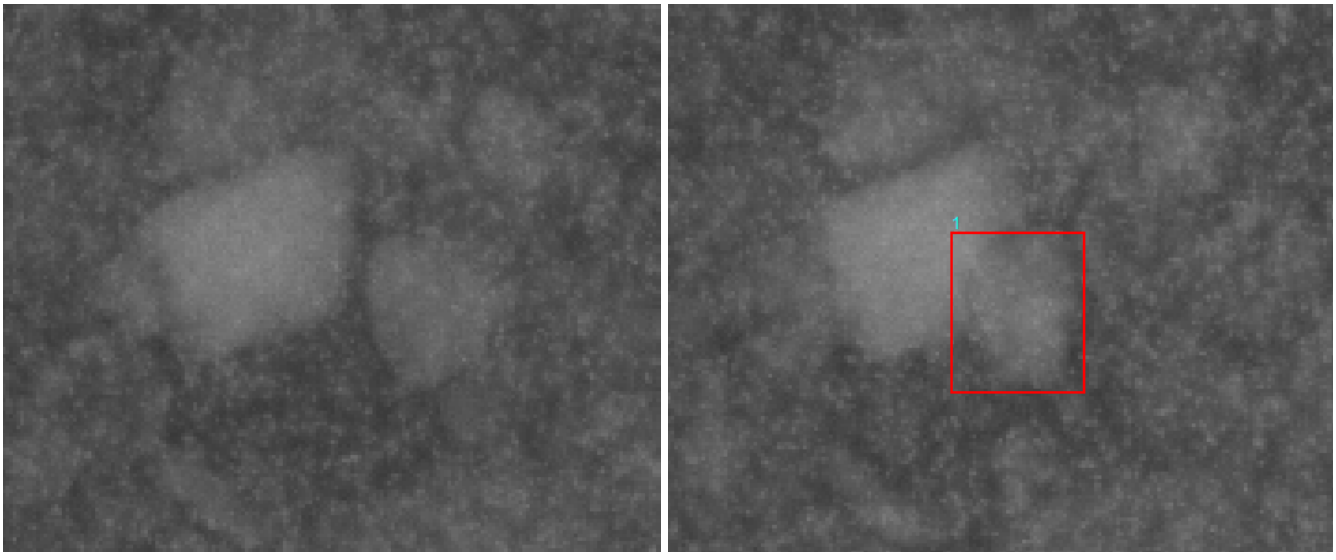

Figure 1.18: Entrainment of a particle

If a particle started or was moving in the previous frame and it is still moving in the current frame, the motion is identified as a “MOVE” (figure 1.17).

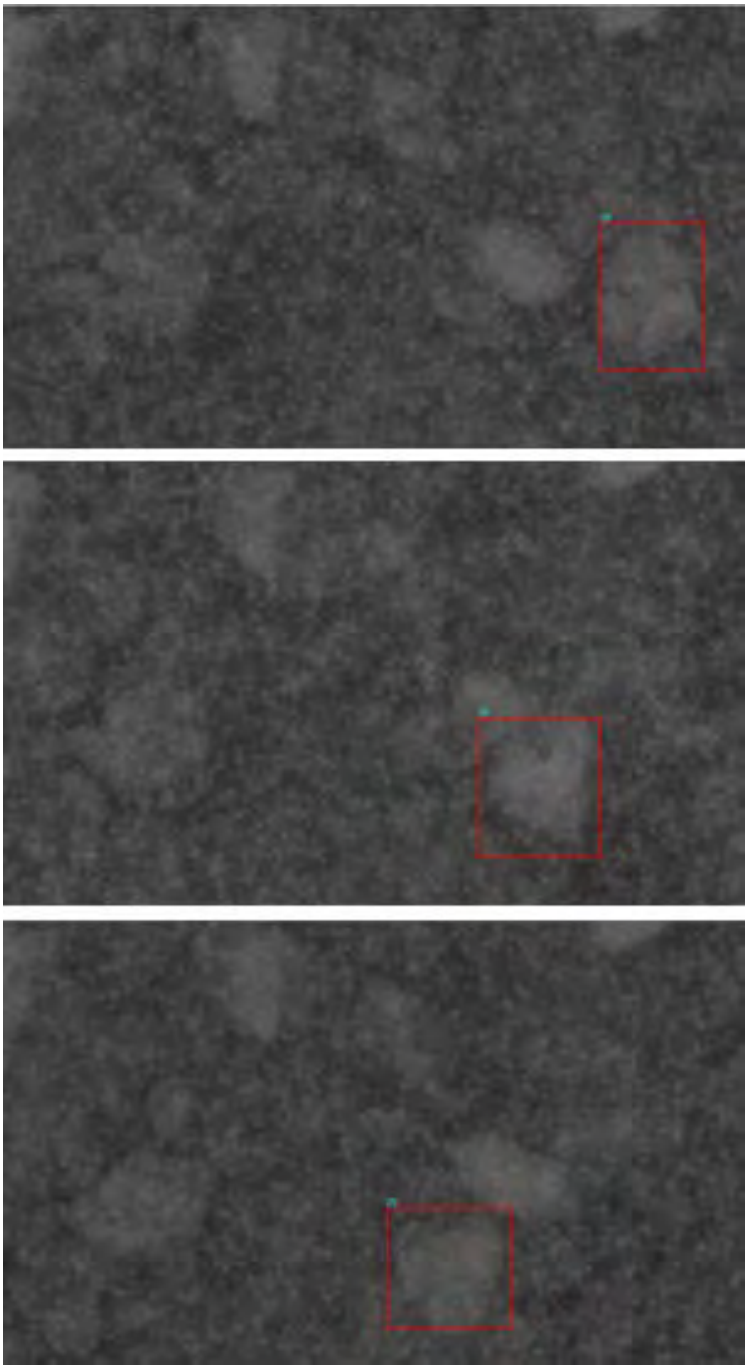

Figure 1.19 : Particle under "move" motion

Finally a "stop" code can be assign to a particle if it rests in its position for more than 0.2 s. Because of the time step between the frames is 0.022 s it was reasonably established that a "stop" was the rest of a particle for almost 10 consecutive frames (figure 1.18).

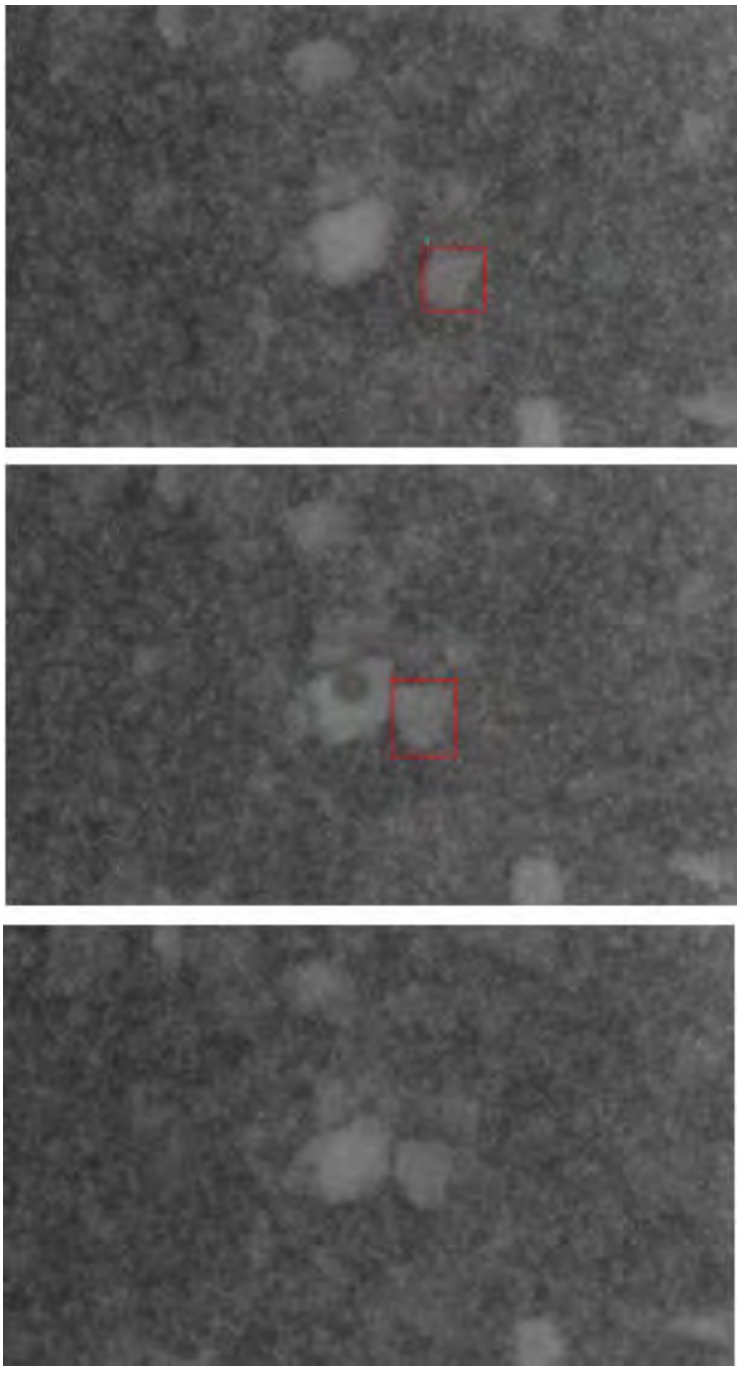

Figure 1.20: Distrainment motion of a grain

At the end of the tracking GSLAB created a structure in which it is possible to know the grains condition for each frame.

Editor - gslab.m | Variables - frame(166).grain

frame(166).grain

frame(166).grain

Fields	number	position	border	area	bbox	state	movedby
1	5	[27.4200 -3....	*2x10 double*	49.8300	[24.1300 -8....	2	[]
2	9	[-61.7000 5....	*2x11 double*	22.7700	[-64.1700 2....	2	[]
3	1	[1.6900 22.0...	*2x10 double*	27.0100	[-1.5500 18....	1	[]
4	137	[89.2600 26....	*2x10 double*	73.0700	[84.5100 21....	2	[]
5	396	[67.6900 -16...	*2x10 double*	54.6800	[62.7600 -20...	2	[]
6							
7							
8							

Figure 1.21: Example of structure for a random frame

Figure 1.19 shows an extract of the database created by GSLAB, specifically reporting the detected grains' situation in correspondence of the frame 166. It is possible to observe how the structure is built focusing on the different columns:

1. Number : it contains the code number of the detected grains that are subjects to any kind of motion in the current frame
2. Position : it files the x and y coordinates of the grain barycentre
3. Border : each row is another structure in which it is possible to collect the coordinates of each point marked outlining the particle's boundary
4. Area : it contains the area of the sediment
5. Bbox : it collects the position of each corner of the bounding box
6. State: it shows the type of motion undergone by the particle in the current frame. In the example particles 5, 9, 137 and 396 are moving, while particle 1 is starting.
7. Movedby : if a particle is moved by another, this last column contains the code number of the hitting grain.

All the identified particles have been memorized by the program. To avoid that an already marked grain was identified as a new one, it was considered that, when a particle was recognized by GSLAB after a certain number of frame:

- it was left the same code number if the number of frame was less or equal to 500. So the particle is identified as the same one.
- The particle was recognized as a new one if the number of frame was greater than 500.

At the end of the data collection the displacement were divided into 5 categories:

- the four categories previously explained start, move, stop, start and stop
- a new category included all the grains that do not start or stop inside the area but with distance lower than window. This means that grains that belonged to this group crosses the investigated area without covering all its length.

Table 1.3: Displacement types for the test made on the 1st October 2009

Start	126
Move	30
Stop	154
Start and Stop	128
Distance lower than a window	73

"Shake" displacements were neglected.
In table 1.3 it is possible to observe the displacement classification for the data base collected by the test developed on the 1st October 2009.

2 Analysis of deposition

The experimental data can be used to explore many different aspects of bedload transport.

The purpose of the study is to investigate the particles distrainment.

"Why a particle stops" is currently a grey area of the sediment transport. That is probably because entrainment and displacement are more attractive: investigating which is the cause of the entrainment, whether the shear stress or the velocity flow field, was the subject of many researchers (Shields 1936, Grass 1970, Wilcock 1993, Scmeeckle et al. 2007, Bottaccin and al. in 2008,). Displacement characteristics, such as length of travel, mode of transport, diffusive patterns in particles' trajectories, have been studied using numerical models too (Drake 1988, Van Rijn 1984). This attention to particles in motion has been legitimised by the need of quantifying the bed-load transport and the aim of linking mathematical formulations to grain's travelling features. Nevertheless, as it is important to understand what the particles entrainment and displacement are due to, the present work's purpose is to understand the reason why, at a point, a particle suspends its motion.

The first issue is to investigate if a reason truly exists, or if the particles distrainment is a completely random process.

To investigate this, a statistical study has been undertaken.

The initial objective is to discover the presence of a correlation between the particles stop positions.

2.1The Poisson process

2.1.1 Theoretical approach

The method used was suggested by another statistical study concerning to the Battle of Britain, that is the name given to the Second World War air campaign waged by the German Air Force against the United Kingdom during the summer and autumn of 1940.

The research goal was to figure out if the bombs were dropped randomly on the territory or if there was a particularly strategy.

The method is based on the Chi Squared test. It is supposed to start stating a null hypothesis (H_0) and an alternative hypothesis (H_1). The hypotheses are stated in such a way that they are mutually exclusive. That is, if one is true, the other must be false, and vice versa.

The hypothesis are:

H_0: the bombs position is completely random

H_1: there is a correlation among the bombs position.

The area was divided into smaller regions. If the position is random the number of bombs placed in each area should have followed a Poisson distribution:

$$p = \frac{e^{-\lambda}\lambda^k}{k!}$$

Where λ is the Poisson parameter, equal to the total number of bombs over the number of regions, and k is the number of bombs per region.

Then it was decided how many categories k it could be good to use. For each category (0 bombs per region, 1 bomb per region…) it was calculated the Poisson probability and the expected number (E_N) of regions by multiplying the probability for the number of regions.

It was also derived the number of regions in which each category k was observed (O_N). Finally dividing O_N for the number of regions the relative frequency was obtained.

It was then possible to calculate the Chi Squared coefficient:

$$\chi^2 = \sum \frac{(O_N - E_N)^2}{E_N}$$

This χ^2 coefficient has to be compared with a reference value. To choose the reference value it is necessary to decide the significant level and to know the degrees of freedom of the distribution. To calculate the degrees of freedom it is enough to subtract the number of constrictions from the number of selected categories k. In this case the constrictions are two:

- The fact that a Poisson distribution is imposed
- The sum of the O_N for each category k must be equal to the sum of the E_N for each category and both must be equal to the number of regions.

If the reference χ^2 is greater than the calculated one, the null hypothesis H_o is true and vice versa.

In the original study it was discovered that the positions in which bombs were dropped were not random. The bombs were more frequently observed nearby the residential areas.

2.1.2 Application

Turning to the particles distrainment, thanks to the tracking it was possible to know the position in which each stop happened.

It was also taken into account the possible restart of a stop particle: the created Matlab code passed through each frame, found out and saved the stops in a matrix. If a grain started again it was deleted from the matrix.

The investigated area, 220 millimetres along the streamwise direction and 80 millimetres in the cross one, was divided into a 22*16 grid. A colourmap was also created for each test to underline the stop density in each area.

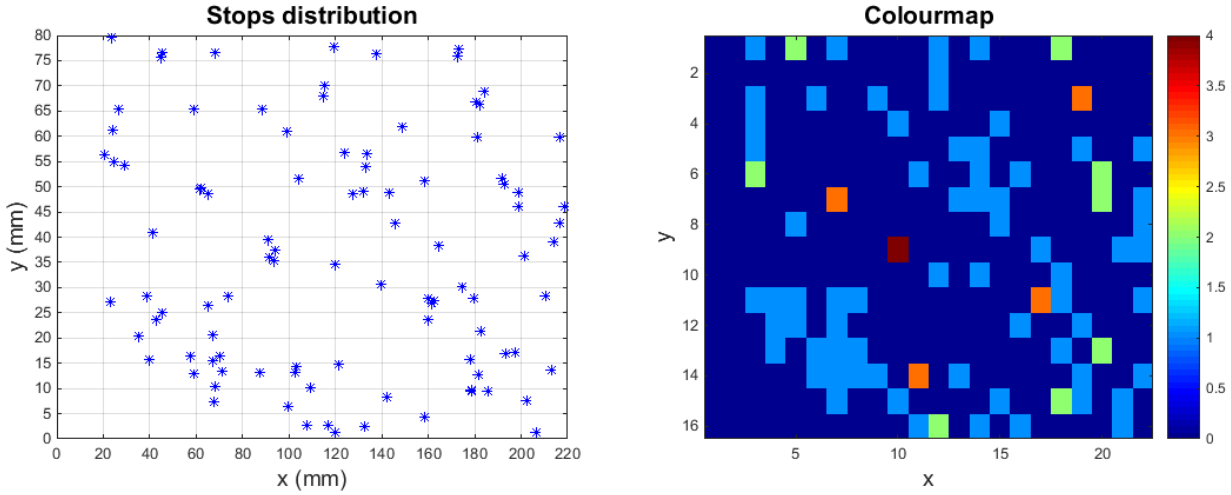

Figure 2.1: Stops distribution in the test of the 24/08, considering all the frames

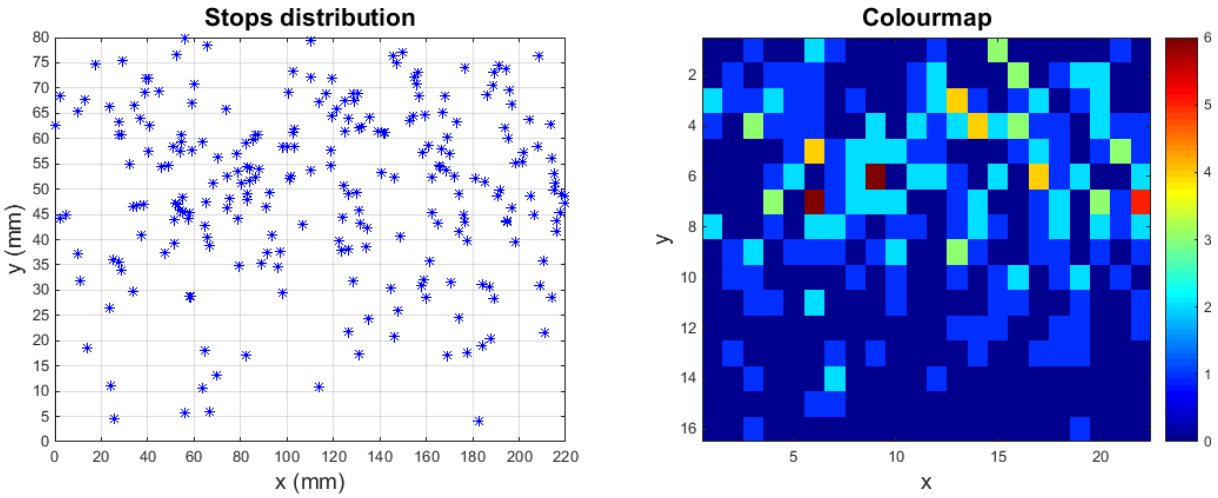

Figure 2.2: Stops distribution in the test of the 02/09, considering all the frames

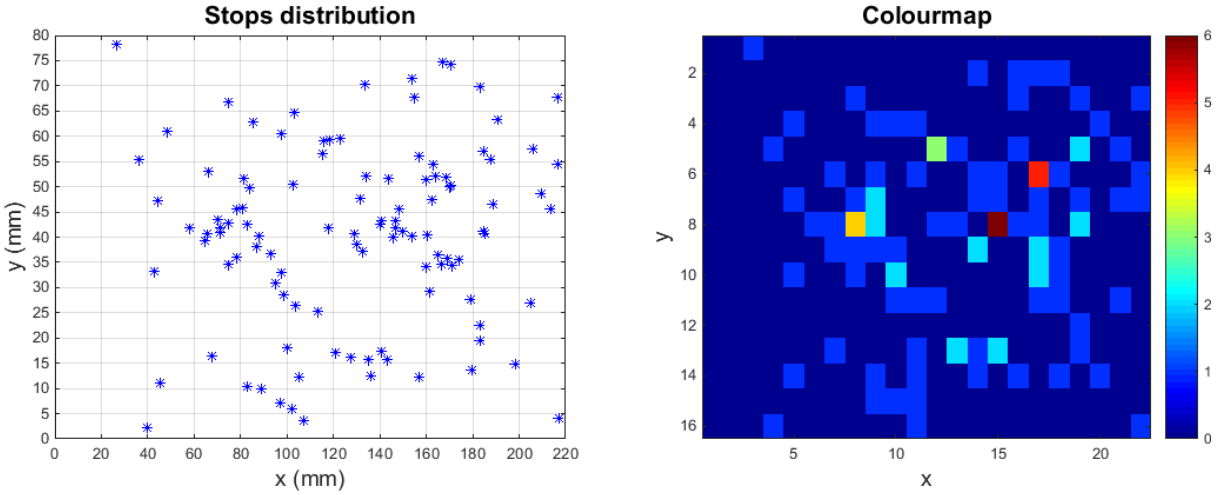

Figure 2.3: Stops distribution in the test of the 22/09, considering all the frames

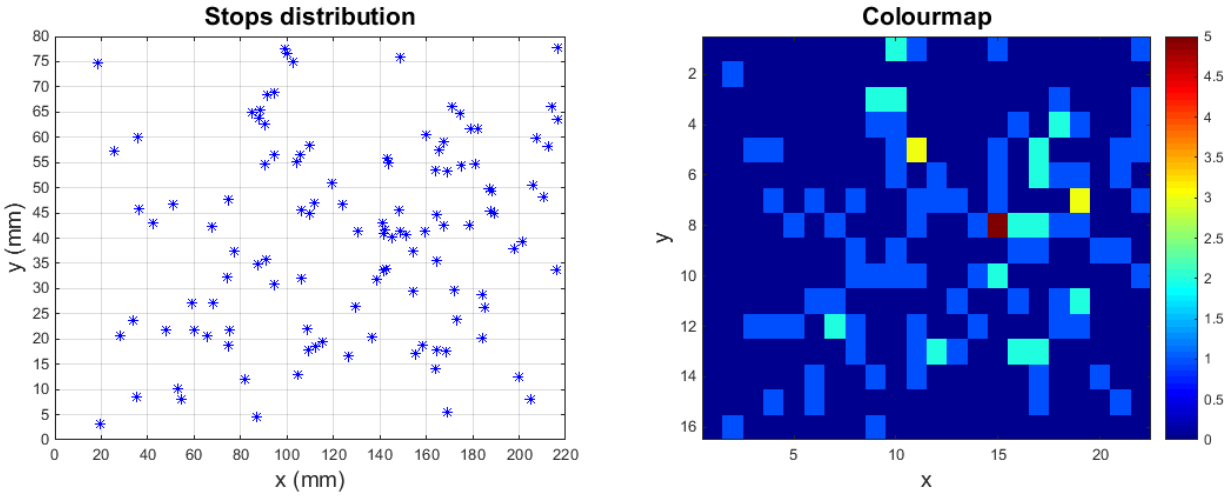

Figure 2.4: Stops distribution in the test of the 23/09, considering all the frames

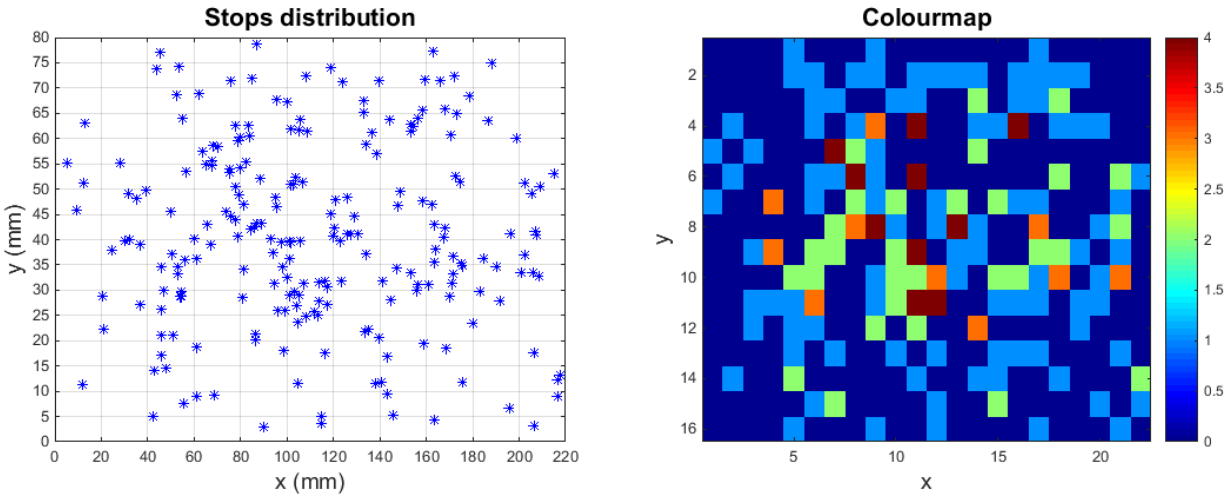

Figure 2.5: Stops distribution in the test of the 29/09, considering all the frames

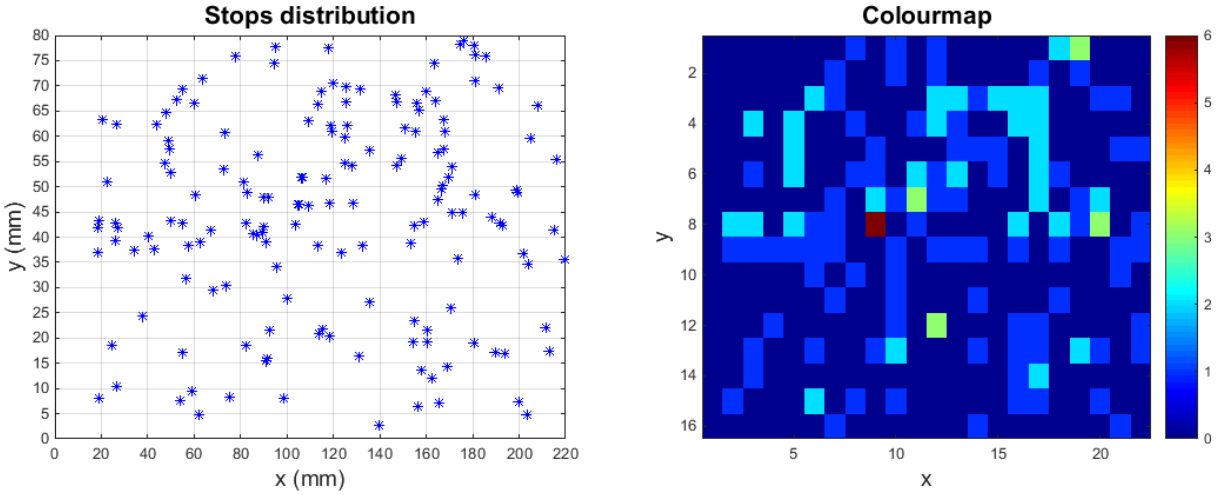

Figure 2.6: Stops distribution in the test of the 01/10, considering all the frames

It was decided to use 10 categories:

- 0 grains per area
- 1 grain per area
- 2 grains per area
- 3 grains per area
- 4 grains per area
- 5 grains per area
- 6 grains per area
- 7 grains per area

- 8 grains per area
- 9 or more grains per area

For this reason the degrees or freedom can be calculated as

$$10\ categories - 2\ constrictions = 8\ degrees\ of\ freedom$$

It was chosen a significant level of 5%.

Using a Chi Squared table is was then easy to find a reference coefficient equal to 15.5.

Percentage Points of the Chi-Square Distribution

Degrees of Freedom	Probability of a larger value of x^2								
	0.99	0.95	0.90	0.75	0.50	0.25	0.10	0.05	0.01
1	0.000	0.004	0.016	0.102	0.455	1.32	2.71	3.84	6.63
2	0.020	0.103	0.211	0.575	1.386	2.77	4.61	5.99	9.21
3	0.115	0.352	0.584	1.212	2.366	4.11	6.25	7.81	11.34
4	0.297	0.711	1.064	1.923	3.357	5.39	7.78	9.49	13.28
5	0.554	1.145	1.610	2.675	4.351	6.63	9.24	11.07	15.09
6	0.872	1.635	2.204	3.455	5.348	7.84	10.64	12.59	16.81
7	1.239	2.167	2.833	4.255	6.346	9.04	12.02	14.07	18.48
8	1.647	2.733	3.490	5.071	7.344	10.22	13.36	15.51	20.09
9	2.088	3.325	4.168	5.899	8.343	11.39	14.68	16.92	21.67
10	2.558	3.940	4.865	6.737	9.342	12.55	15.99	18.31	23.21
11	3.053	4.575	5.578	7.584	10.341	13.70	17.28	19.68	24.72
12	3.571	5.226	6.304	8.438	11.340	14.85	18.55	21.03	26.22
13	4.107	5.892	7.042	9.299	12.340	15.98	19.81	22.36	27.69
14	4.660	6.571	7.790	10.165	13.339	17.12	21.06	23.68	29.14
15	5.229	7.261	8.547	11.037	14.339	18.25	22.31	25.00	30.58
16	5.812	7.962	9.312	11.912	15.338	19.37	23.54	26.30	32.00
17	6.408	8.672	10.085	12.792	16.338	20.49	24.77	27.59	33.41
18	7.015	9.390	10.865	13.675	17.338	21.60	25.99	28.87	34.80
19	7.633	10.117	11.651	14.562	18.338	22.72	27.20	30.14	36.19
20	8.260	10.851	12.443	15.452	19.337	23.83	28.41	31.41	37.57
22	9.542	12.338	14.041	17.240	21.337	26.04	30.81	33.92	40.29
24	10.856	13.848	15.659	19.037	23.337	28.24	33.20	36.42	42.98
26	12.198	15.379	17.292	20.843	25.336	30.43	35.56	38.89	45.64
28	13.565	16.928	18.939	22.657	27.336	32.62	37.92	41.34	48.28
30	14.953	18.493	20.599	24.478	29.336	34.80	40.26	43.77	50.89
40	22.164	26.509	29.051	33.660	39.335	45.62	51.80	55.76	63.69
50	27.707	34.764	37.689	42.942	49.335	56.33	63.17	67.50	76.15
60	37.485	43.188	46.459	52.294	59.335	66.98	74.40	79.08	88.38

Figure 2.7: Chi Square table

The test was repeated considering an increasing number of frames:

- From frame 1 to frame 1000, 22 seconds
- From frame 1 to frame 2000, 44 seconds
- From frame 1 to frame 3000, 66 seconds
- From frame 1 to frame 4000, 88 seconds
- From frame 1 to frame 5000, 110 seconds
- From frame 1 to the final frame, 132 seconds ish.

The results are presented in table 2.1

Table 2.1: Chi square test

Test 3	
Seconds	χ^2
22	0.2
44	0.0
66	5.1
88	23.5
110	23.3
132	22.8

Test 5	
Seconds	χ^2
22	0.3
44	10.3
66	153.0
88	79.7
110	58.5
132	154.6

Test 9	
Seconds	χ^2
22	0.2
44	425.0
66	128.0
88	999.1
110	435.1
132	3331.3

Test 10	
Seconds	χ^2
22	6.3
44	14.6
66	7.6
88	107.4
110	111.8

Test 11	
Seconds	χ^2
22	5.2
44	34.8
66	9.3
88	69.2
110	87.5
132	72.9

Test 12	
Seconds	χ^2
22	0.4
44	3.3
66	257.7
88	1595.0
110	738.4
132	357.4

The red numbers are the ones that are lower than the reference coefficient 15.5 and hence the ones that state a random distribution.

The values greater than 15.51 define that the stop distribution cannot be assumed as a random process.

It has always been found that for a small amount of frames (1000) the locations turned out to be random.

On the contrary, when the whole number of frames was taken into account, the χ^2 was always greater than 15.81.

This result bring to the hypothesis that stop particles probably star to be correlated with time, clustering around previous stops. This is probably due to the local change in the bed elevation, caused by a grain deposition, that increase the probability for the following particles to stop too.

2.2 Temporal autocorrelation

Since the Chi Square test stated a spatial correlation, an autocorrelation procedure was carried out to understand if a variable is cross-correlated with itself at different times. The aim was to find out if the correlation was only spatial or either temporal. Because of the autocorrelation formula, in which mean and standard deviation are needed, it was decided to calculate the autocorrelation coefficient for the distances between particles.

The definition of the autocorrelation between times s and t is:

$$R(s,t) = \frac{E[(d_t - \mu_t)(d_s - \mu_s)]}{\sigma_t \sigma_s}$$

The coefficient can vary between -1, if the value has a perfect anti-correlation, and 1, with a perfect correlation. If the value of the coefficient is close to zero, it means that there is no autocorrelation.

Since it was necessary to have the mean values at different times it was decided to analyse the autocorrelation between groups of 5 stop particles. The groups were created just following a chronological order: when the first 5 stops had been found, they generated the first group. For this first pack, the mutual distances between the particles has been found and a mean distance value was obtained.

The same procedure, illustrated in figure 2.8, was carried out with the second cluster of 5 stops and then the two consecutive groups were linked gaining the autocorrelation coefficient.

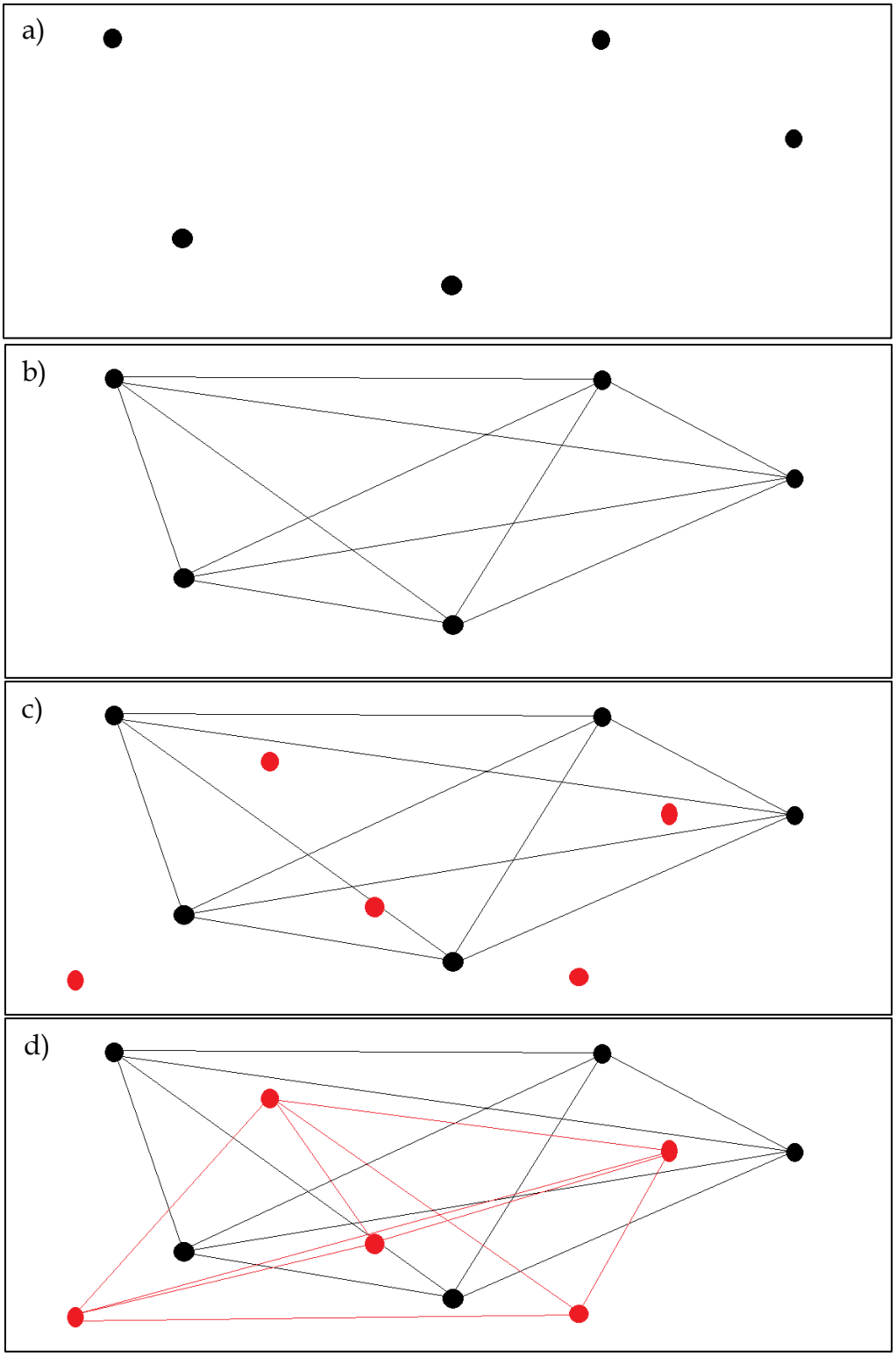

Figure 2.8: Autocorrelation procedure: a) arrival of 5 stops b) calculation of the distances c) arrival of other 5 stops d) calculation of the distances

The procedure was repeated for all the groups of 5 stops, until the end of each test.

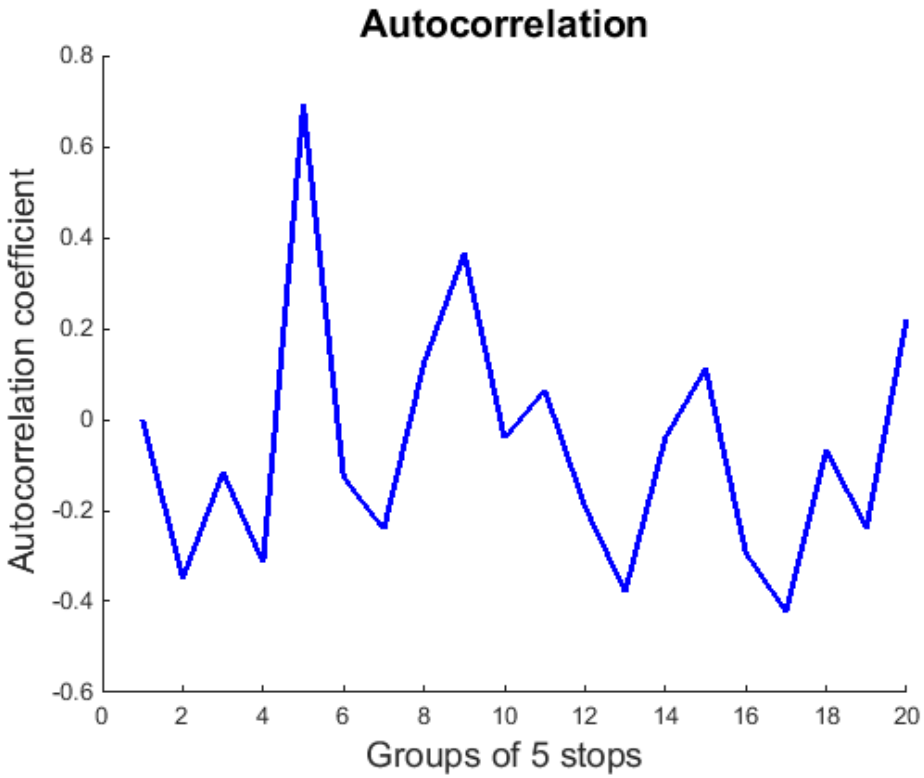

Figure 2.9: Autocorrelation in the test of the 24/08

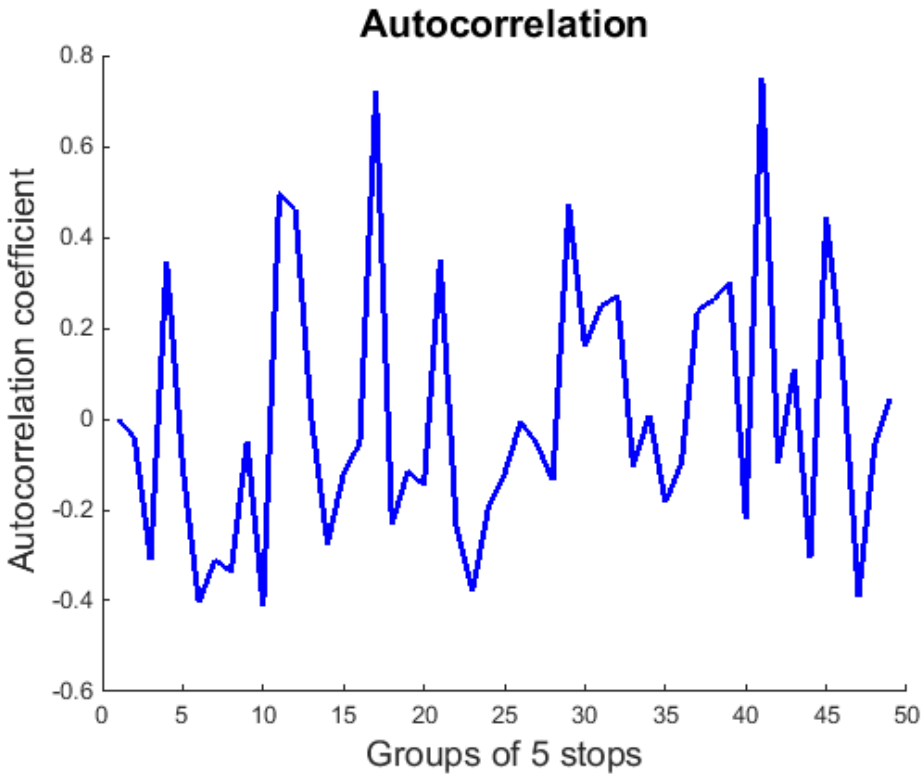

Figure 2.10: Autocorrelation in the test of the 02/09

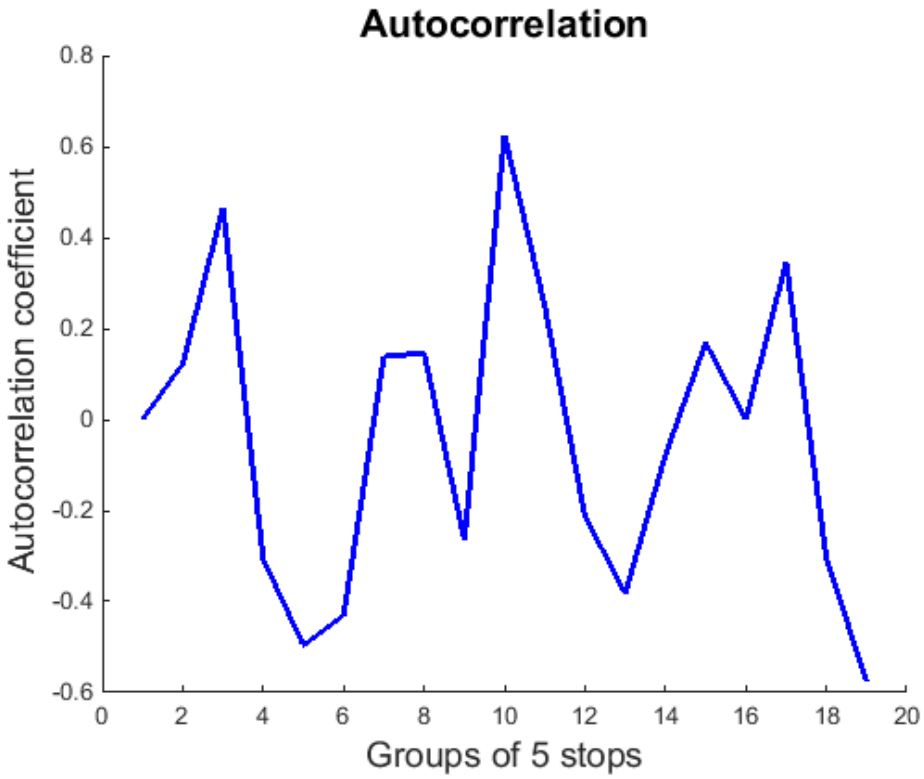

Figure 2.11: Autocorrelation in the test of the 22/09

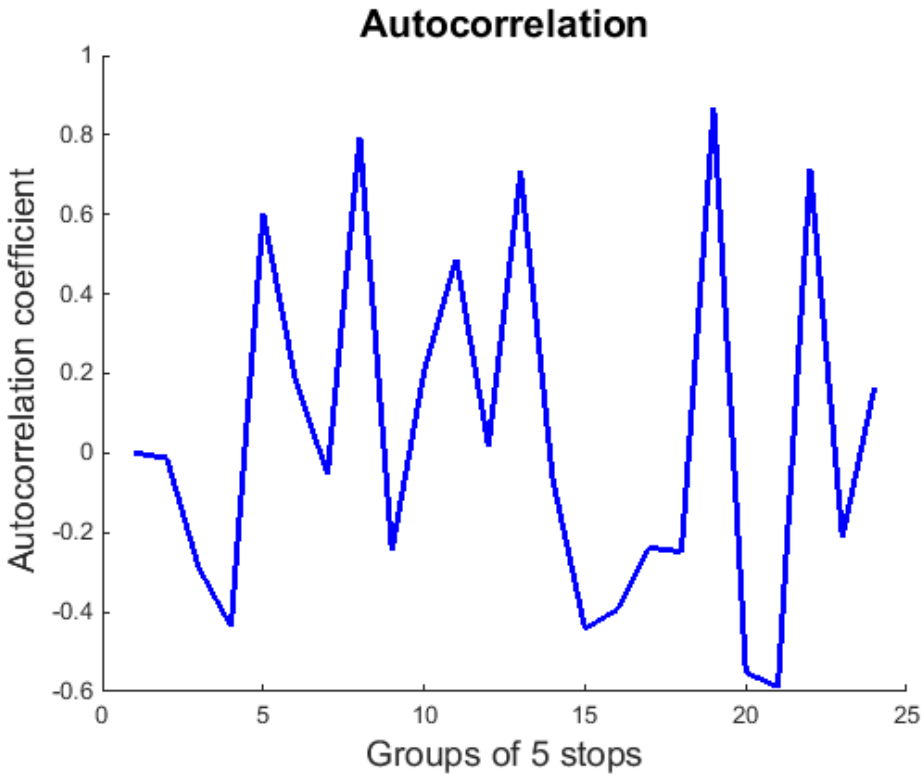

Figure 2.12: Autocorrelation in the test of the 23/09

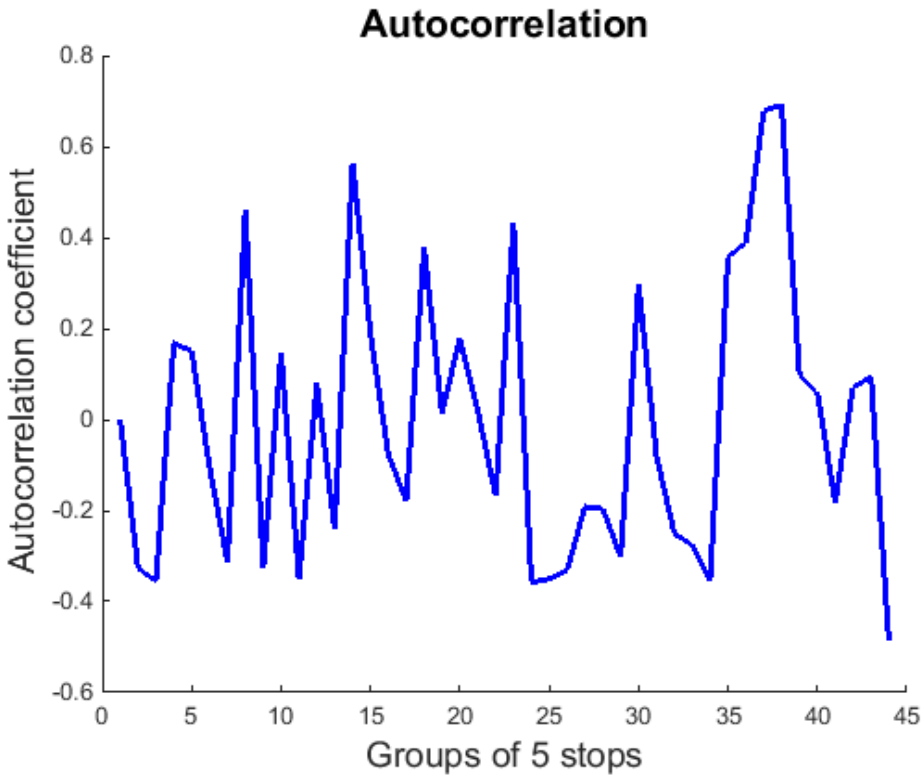

Figure 2.13: Autocorrelation in the test of the 29/09

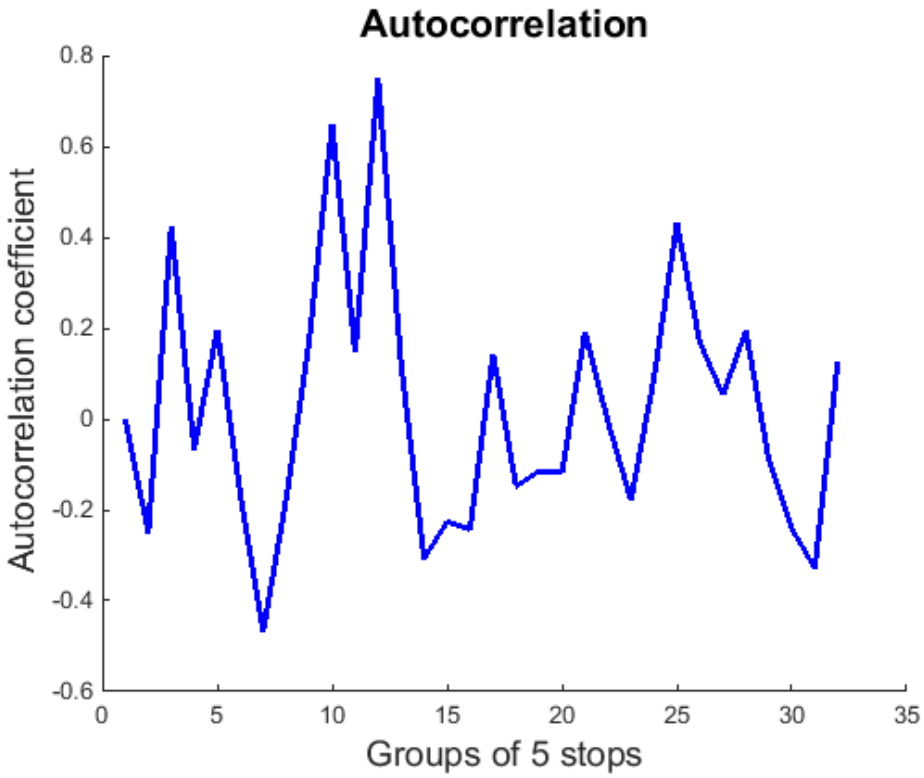

Figure 2.14: Autocorrelation in the test of the 01/10

The tests revealed that the autocorrelation coefficient is at least equal to 0.86, but just one sporadic episode and with a mean value close to zero for each test, as shown in table 2.2.

Table 2.2: mean, max and min autocorrelation coefficient for each test

Test	Mean coefficient	Max coefficient	Min coefficient
24/08/2009	-0.0621	0.6909	-0.4225
02/09/2009	0.0065	0.7488	-0.4129
22/09/2009	-0.0425	0.6252	-0.5766
23/09/2009	0.0407	0.8692	-0.5876
29/09/2009	-0.0065	0.6909	-0.4884
01/10/2009	0.0228	0.7492	-0.4677

For most of the time the coefficient fluctuates around zero. This probably happens because the analysis considers 5 stops taken in chronological order but that can deposit in completely different parts of the area. The fact that the stop process is not random does not mean that the clusters have been created in a precise sequence.

2.3 Distances between stops

Since the chronological analysis does not brought to any significant results, the distance between particles can also be investigated just from a spatial point of view, looking at a sort of spatial autocorrelation. The problem was developed first creating a structure: for each single particle it was calculate the distance with all the other particles. The distances were studied with a frequency analysis in order to find a significant distance d. This distance has following property: if a distance between two particles is less than d, that particle influence each other's position, on the contrary if their distance is greater than d their position is absolutely independent.

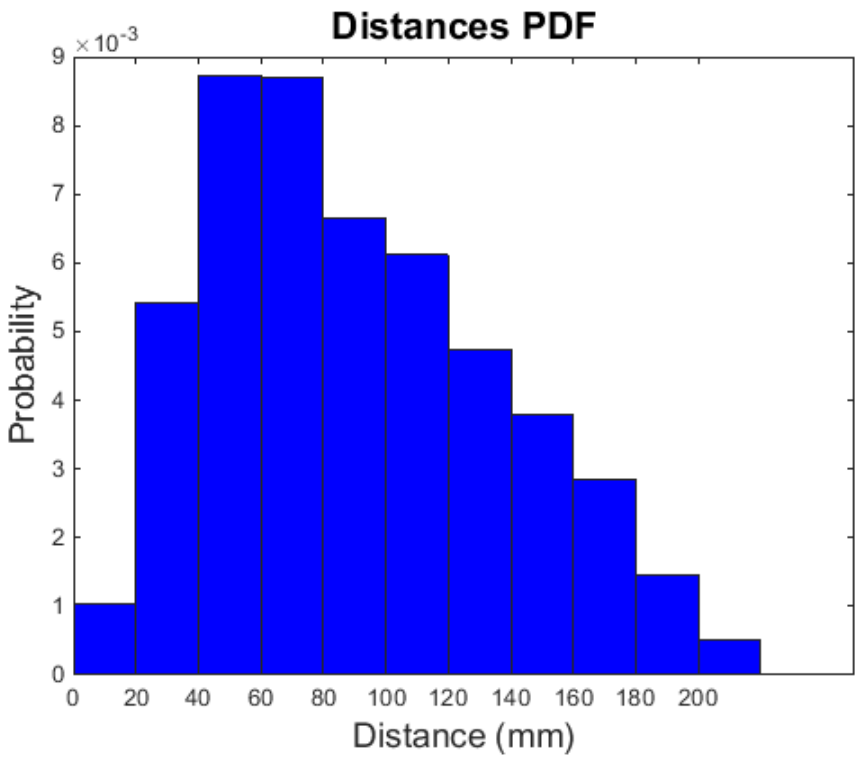

Figure 2.15: PDF of the distances in the test of the 24/08

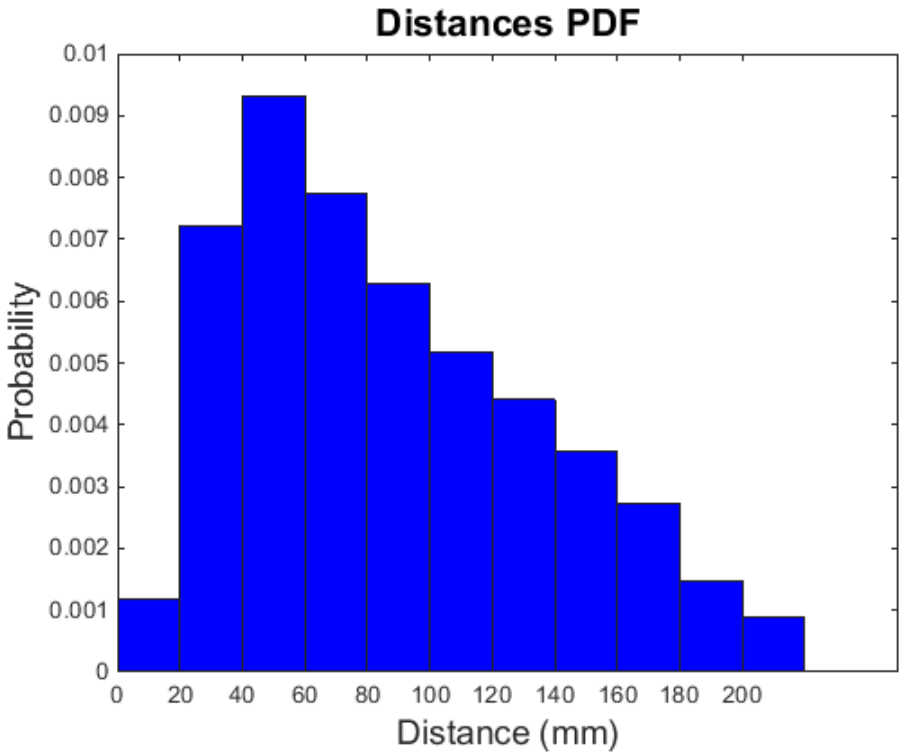

Figure 2.16: PDF of the distances in the test of the 02/09

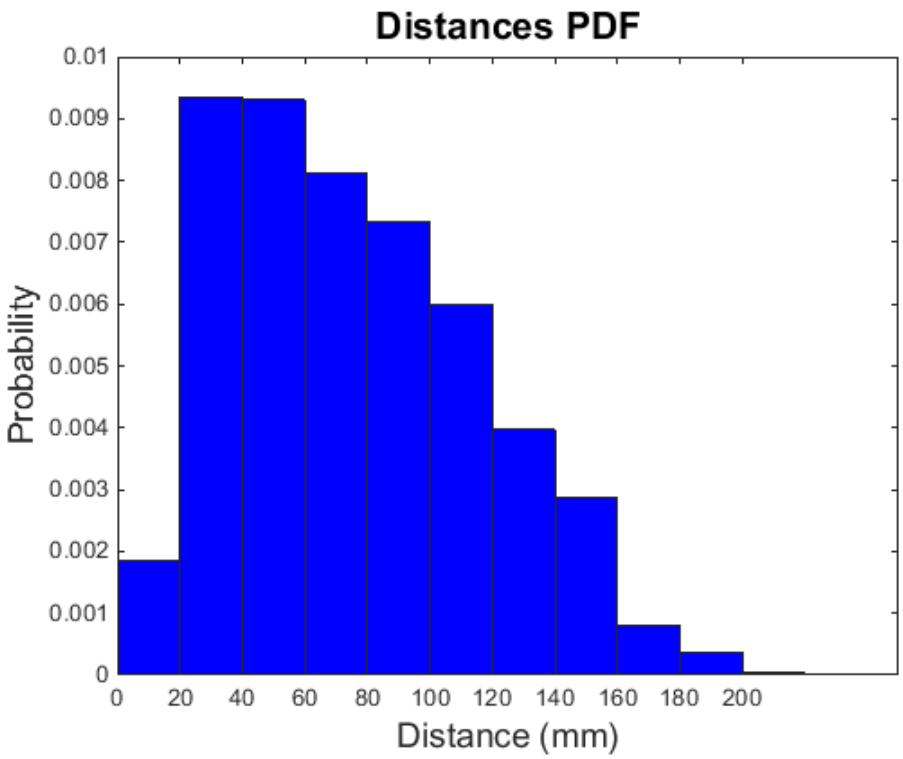

Figure 2.17: PDF of the distances in the test of the 22/09

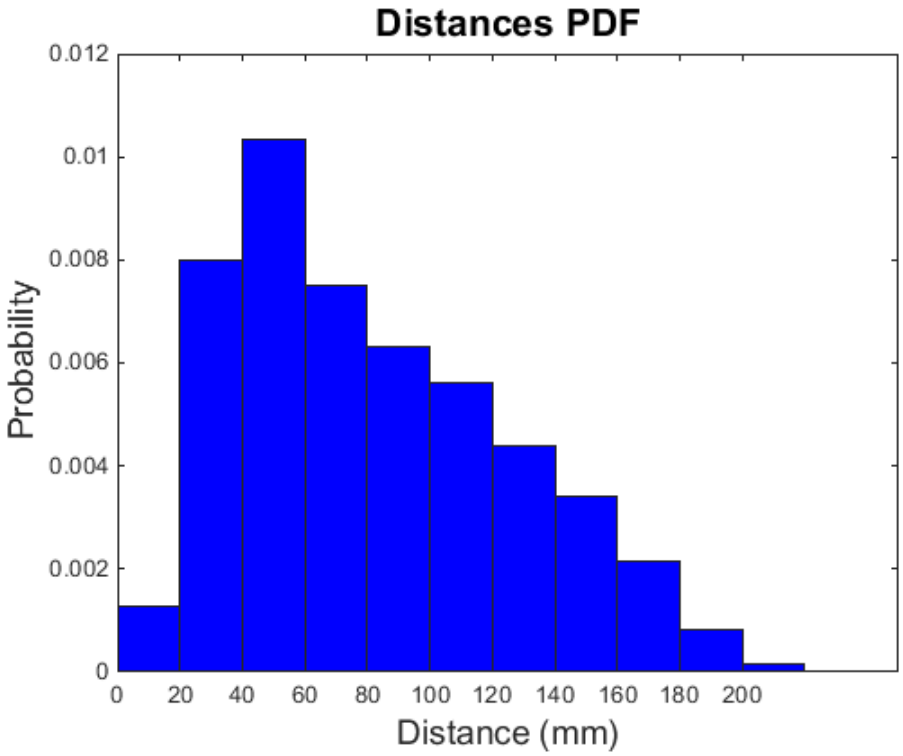

Figure 2.18: PDF of the distances in the test of the 23/09

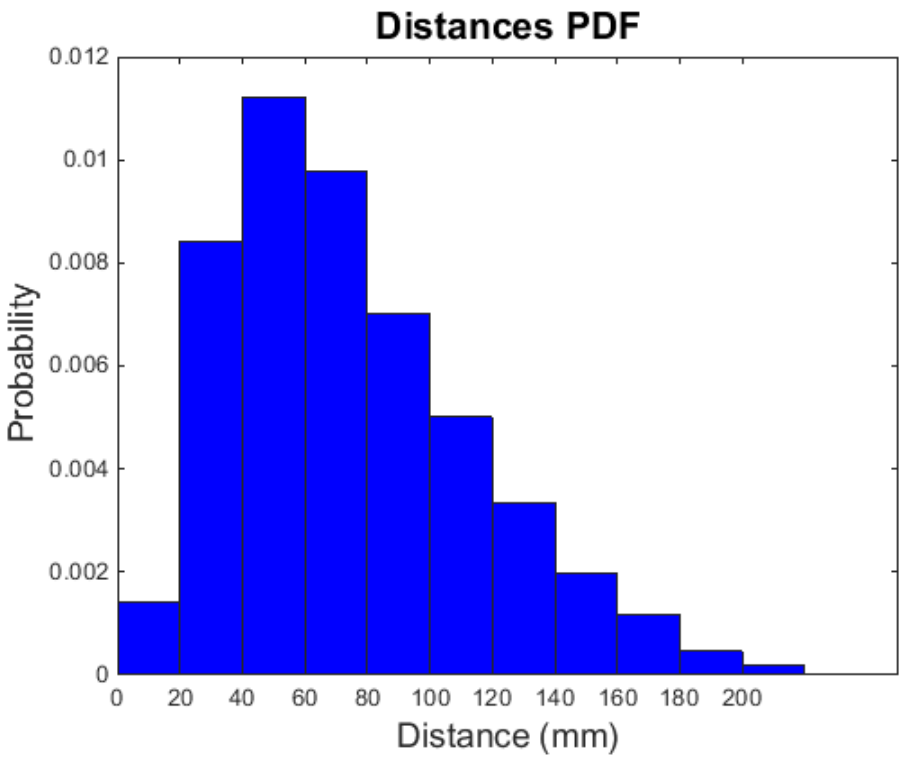

Figure 2.19: PDF of the distances in the test of the 29/09

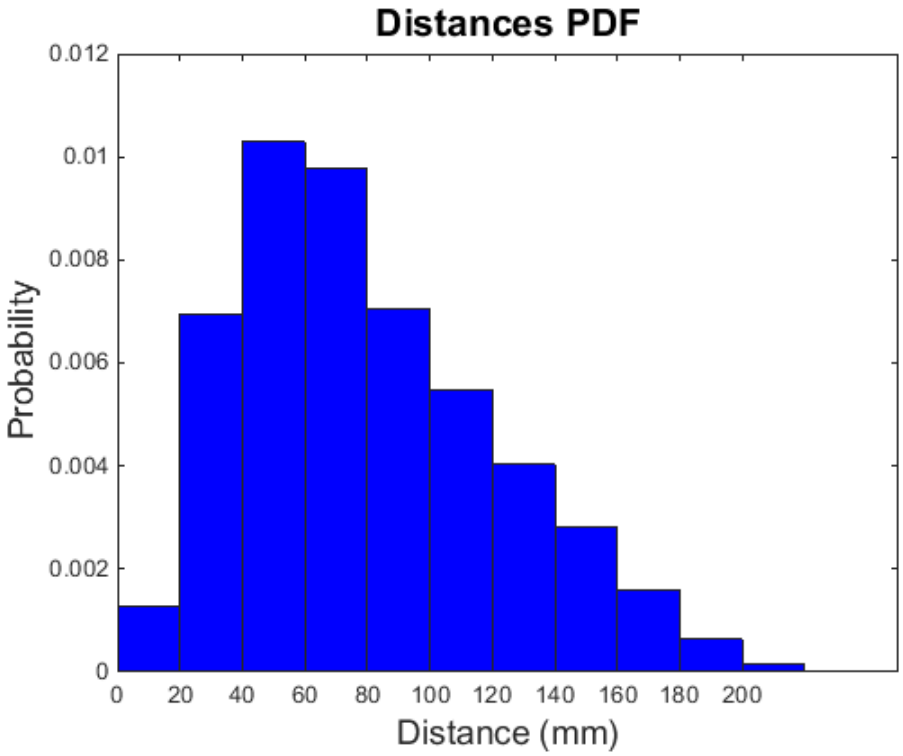

Figure 2.20: PDF of the distances in the test of the 01/10

Looking at the histograms it is possible to see that the most frequent distance varies between 40 and 60 millimetres, apart from the test of the 22nd of September, in which there is a slightly higher frequency in the interval 20-40 mm. The PDFs were created considering all the frames, but the same result was obtained also varying the temporal interval.

The distances analysis has not led, again, to satisfactory results, hence it is necessary to tray with another spatial autocorrelation analysis.

2.4 Spatial autocorrelation

Given that the Poisson process and its linked plots show the presence of clusters of stops, it was tried to verify if a cluster analysis could identify them.

According to Anselin (1980), spatial autocorrelation can be defined as a spatial cluster of comparable parameters values. A nearness of similar parameters values gives a positive autocorrelation, on the contrary a nearness of dissimilar parameters values gives a negative autocorrelation.

In statistics spatial autocorrelation is investigated using the Moran coefficient and the Gaery coefficient.

The Moran coefficient can be defined as follow:

$$M = \frac{N}{\sum_i \sum_j W_{ij}} \frac{\sum_i \sum_j W_{ij} (x_i - \bar{x})(x_j - \bar{x})}{\sum_i (x_i - \bar{x})^2}$$

where W_{ij} is a spatial weight equal to 1 for neighbouring cells and 0 otherwise, N is the number of geographic units, x_i is the variable that describes the analysed phenomenon and $\bar{x}$ is its mean. M can range between -1 and 1, indicating negative spatial autocorrelation for values close to -1, no spatial correlation for M=0, and high positive spatial correlation for M close to 1.

Similarly, the Gaery coefficient is calculated as:

$$G = \frac{N-1}{\sum_i \sum_j W_{ij}} \frac{\sum_i \sum_j W_{ij} (x_i - x_j)^2}{2 \sum_i (x_i - \bar{x})^2}$$

Differently from the Moran coefficient, Gaery coefficient ranges between 0 and 2. If the coefficient is equal to 0 there is positive autocorrelation , if the coefficient is equal to1 there is no correlation, if the coefficient is equal to 2 there is negative autocorrelation.

Table 2.3: Moran and Gaery coefficients in the first 1000 frames for each test

	Moran	Gaery
24/8	-0.0265	1.0331
2/9	0.0743	0.9146
22/9	-0.0232	1.0052
23/9	0.0146	1.0108
29/9	0.0240	1.0112
1/10	0.0309	0.9932

Table 2.4: Moran and Gaery coefficients in all the frames for each test

	Moran	Gaery
24/8	0.048	0.9541
2/9	0.1671	0.8352
22/9	0.127	0.9033
23/9	0.091	0.9268
29/9	0.1971	0.8306
1/10	0.103	0.9152

Both Moran and Gaery coefficient have been derived for all the tests and for different frames, but without providing significant results. The maximum value for the Moran coefficient was 0.19, very close to zero denoting the absence of spatial autocorrelation. The Gaery coefficient confirmed the random spatial distribution.

It is also interesting to notice how the Moran coefficient increases over time. This confirms what was found with the Poisson test: the stops position could depend on the bed roughness. Moran and Gaery coefficients are commonly used with geographical measurements, such as population density. It is true that a grain that stops on the bed can influence other grains,

stopping them by collision or increasing bed elevation, but it is also true that this does not influence nearby areas. In particular, the bigger the cell size with respect to the grain dimension, the more random the process appears within nearby areas.

The conclusion that can be deduced from the plots and the stops analysis is that there is a not random process that is more and more likely with the passing of time.

This probably happens because the deposition of particles occurs in time, changing the bed elevation and this will influence the deposition of the following particles nearby.

The limit is that it is not possible to monitor the process longer, because the analysis, very energy expensive, was undertaken only on the first 6000 frames.

3 Deposition-velocity correlation

The Poisson test, as showed before, stated that the disposition of the stop particles is definitely a not-random process. After the first frames period indeed, where particles seem to stop without any mutual influence, the distrainment process appear to happen in spatial clusters. As seen before in fact, the particles disposition seems more likely to occur in some part of the bed, more than in other.

As a consequence, it is interesting to find out which variables the stops location is dependent on.

The variation of the χ^2, Moran and Gaery coefficients over time, suggests that there could be a correlation between the particles spatial distribution and the bed roughness.

Unfortunately in the Bradford tests, instantaneous and local values of bed elevation and its fluctuation were not measured.

But since the PIV data was available for the three tests of the 24th of August, 2nd of September and 22nd of September it was suitable to verify the possible correlation between stops position and the velocity flow field, since.

3.1 The PIV data

The available velocity data was very complex because it consists of a four dimensions matrix: velocity changes both in space (x, y, z dimensions) and in time.

The planar area covered by the PIV was divided into a thick mesh, with 185 nodes along the streamwise direction and 35 nodes along the cross direction, where the velocity was known.

Unfortunately not all the nodes had the same mutual distance, in particular in the edges of the investigated area. Because of this, only the central part of the mesh was considered, where the cells were all 1.2*1.3 mm^2, obtaining 180*28 nodes and, consequently, a spatial matrix with the same size for each frame.

The total surface of the considered investigated area was a little bit different for each test but always about 22.5*3.18 cm^2.

From a temporal point of view, one matrix for each frame was available. It was decided to reduce them applying a time average to groups of 100 matrices, covering 2.2 seconds per matrix.

Because the PIV area is smaller than the whole analysed area, it was necessary to reduce to the same size also the matrix that contains all the stops position, so then it would be possible to overlap the two.

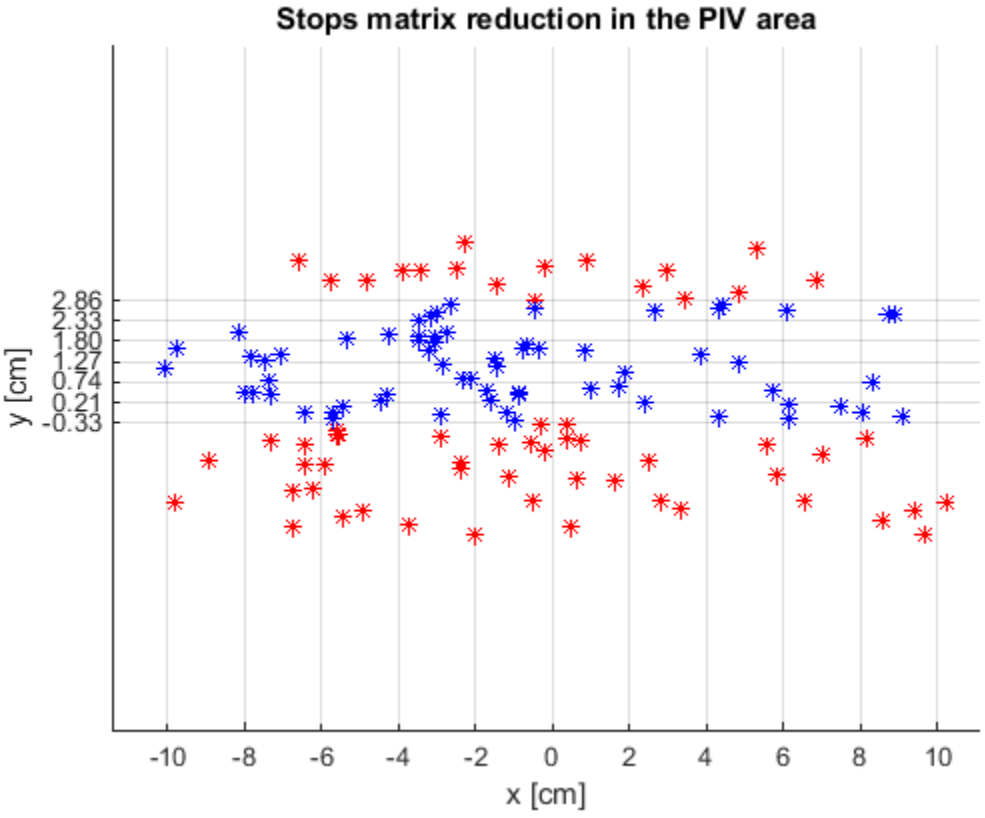

Figure 3.1: Stops location plot that shows the reduced stops matrix

3.2 Areas of averaged velocity

Once derived the PIV data it was decided to create a contour plot. A contour plot is "*a graphical technique for representing a three dimensional surface by plotting constant z slices, called contours, on a two dimensional format. That is, given a value for z, lines are drawn for connecting the (x,y) coordinates where that z value occurs*" (Engineering Statistics Handbook).

The "z" value in the analysed case is the velocity, plotted in the two dimensional area for a specific group of frames.

The plot was created with the idea to have a first visualization of a likely or not link between stops and velocity.

Every slice is coloured according to the velocity order of magnitude as reported in the adjacent coloured bar.

If the two variables were linked, it would be expected that the two variables would follow the same patterns, hence a prevalence of stops in the regions where the velocity is lower, where the blue in the images is darker, or where the velocity is higher, where the images are coloured in yellow.

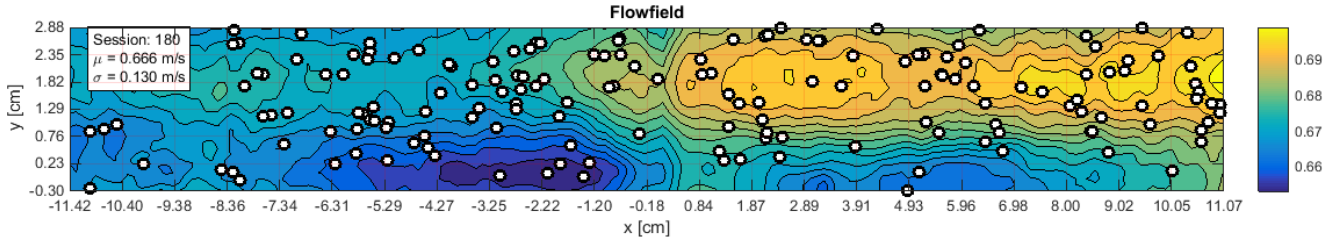

Figure 3.2: Contour plot for the test of the 02/09, considering all the frames

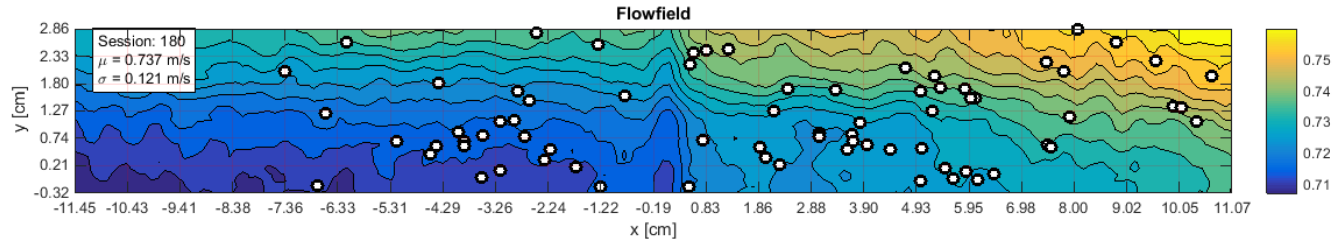

Figure 3.3: Contour plot for the test of the 22/09, considering all the frames

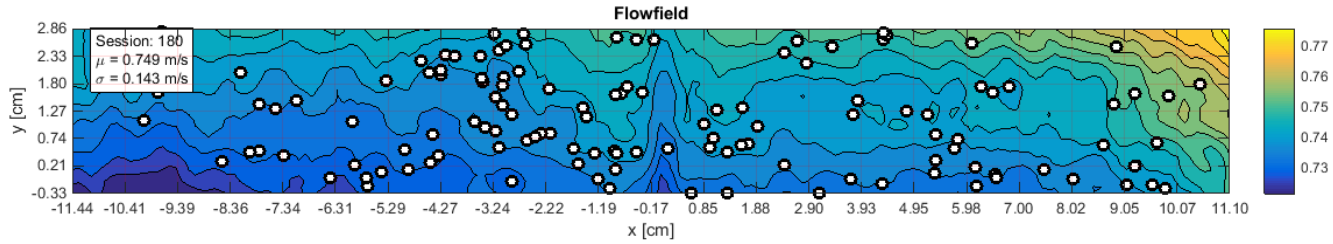

Figure 3.4: Contour plot for the test of the 29/09, considering all the frames

Even if this analysis does not produce any quantifiable results about correlation, the plots do not seem to show a clear link between the stops location and the velocity flow field.

3.3 Spatial and temporal Average

To analytically compare the stops and the velocity field, it is necessary to reduce them to the same geometrical conditions.

The PIV investigated area and the now equivalent deposition area have been both divided into a 22*6 grid.

Since the whole area is about 22.5*3.18 cm^2, every knit is around 10 millimetres long in the streamwise direction and 5 millimetres long in the cross one. This size was chosen to considered about the size of two grains along the stramwise direction and of one grain in the cross one.

The PIV velocity data, that was already averaged in time for groups of 100 frames, was also averaged over the bed.

It was written a Matlab code able to calculate a mean velocity that was averaged on the basis of the cells-subdivision decribed before.

It is now possible again to create a plot that compares the stops position with the double averaged velocity over the grid.

Figures from 3.5 to 3.7 show the double averaged velocity with different colour intensities and in white the stops locations.

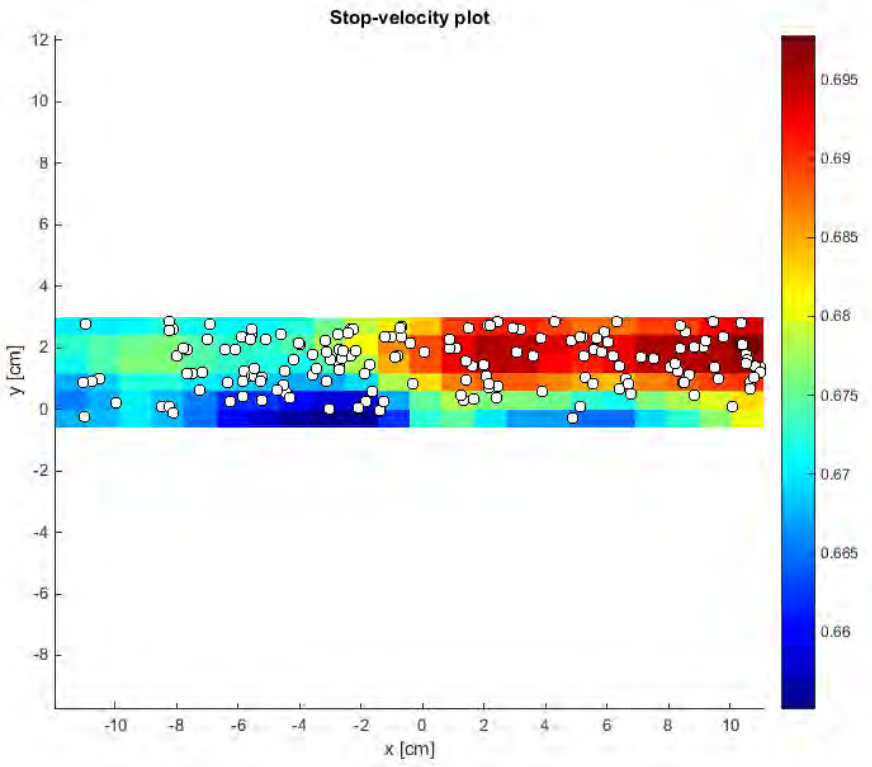

Figure 3.5: Plot that compares the stops position and the double averaged velocity in the test of the 02/09, considering all the frames

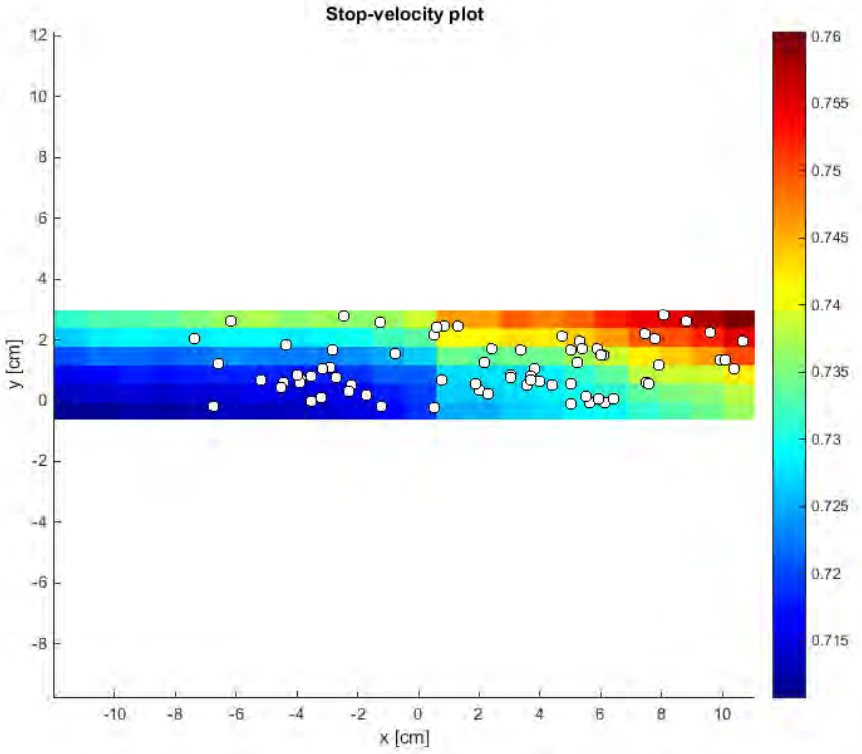

Figure 3.6: Plot that compares the stops position and the double averaged velocity in the test of the 22/09, considering all the frames

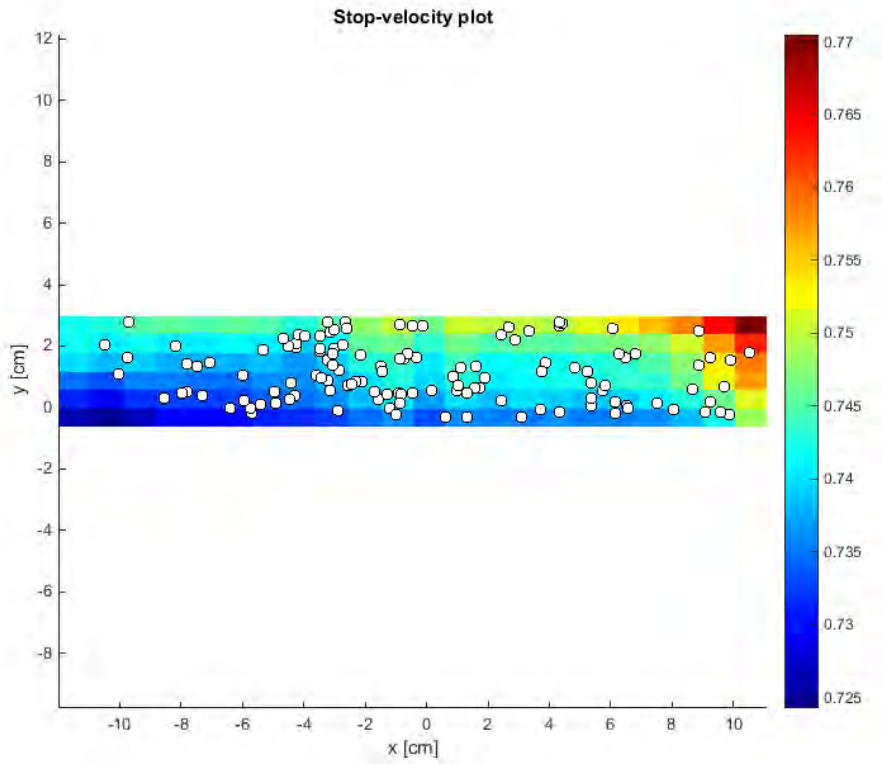

Figure 3.7: Plot that compares the stops position and the double averaged velocity in the test of the 29/09, considering all the frames

Again the visual inspection does not give any idea of correlation between the two physical quantities, but it is scientifically important to prove it by calculating the statistical correlation coefficient between the variables.

3.4 Stops-velocity correlation

Since two matrices of the same size and geometrical configuration are now available, it is possible to deal with a correlation coefficient calculation.

With respect to the stops, the number of distrainment was counted for each knit, without considering, as in the previous analysis, the stops that eventually would restart later.

The number of stops was then divided by the area of the knit, to find out a stop density number.

Just to remember some theoretical aspects, the correlation formula is shown below:

$$R = \frac{\sum_{i=1}^{n}(x_i - \mu_x)(v_i - \mu_v)}{\sqrt{\sum_{i=1}^{n}(x_i - \mu_x)^2}\sqrt{\sum_{i=1}^{n}(v_i - \mu_v)^2}} = \frac{\sigma_{xv}}{\sigma_x \sigma_v}$$

where x_i and v_i are, respectively, the stop density value and the double averaged velocity in the i^{th} knit, μ_x and μ_v are the mean for the two quantities and σ_x, σ_v and σ_{xv} are the standard deviation.

The correlation is positive or direct, when the variation of the two quantities is directly proportional; it is negative, indirect or inverse, when the quantities are inversely proportional. Correlation is then "simple", when only two physical magnitudes are compared, as in the present study; it is double when there are three phenomena, triple with four and so on.

The degree of correlation is stated by the correlation coefficient. It can vary between -1 and 1. The coefficient is equal to 1 when the two variables are perfectly directly correlated; it is equal to -1 when the two are perfectly indirectly correlated; it is finally equal to 0 when there is the absolute absence of correlation. Two independent variables have, for sure, a null correlation coefficient.

In the present study the correlation coefficient was calculated for each one of the three tests for which the PIV data was available, for different groups of frames.

Table 3.1: Correlation coefficients

Seconds	Test 5	Test 9	Test 11
22	0.0796	0.1242	-0.1187
44	0.0322	-0.0538	-0.0722
66	0.0399	-0.1124	-0.1469
88	0.1791	-0.0079	-0.1149
110	0.1769	-0.0195	-0.1431
~132	0.1916	0.0187	-0.1225

The coefficient is always extremely low, almost equal to zero. To have a second validation, the correlation procedure was repeated considering the number of stops for each cell, instead

of the stop density, but, since they differ only for a constant quantity, the obtained coefficients were exactly the same.

This states the total lack of correlation between the stops density and the velocity field.

In other words velocity seems to be absolutely independent from the deposition phenomenon.

The absence of correlation leads to the conclusion that maybe the stop particles are linked with the bed elevation evolution, but unfortunately data set about roughness is not available for these tests series.

Probably new different experiments could be done to validate or not this theory, measuring detailed bed topography at various stages.

Conclusions

Bedload transport has been a research subject for years. Nevertheless the mechanics of deposition have marginally been investigated. Sediment transport is highly influenced by deposition: the dead zones and the polluted sediments accumulation in some areas of the riverbed are only some of the possible examples.

The absence of previous studies has often brought to some difficulties in approaching the distrainment problem and the lack of comparison possibilities with previous analyses still leaves lots to say about the cease of motion.

The experiment carried out in Bradford in 2009, not entirely analysed yet, still provide a rich database of the individual particles motion. Besides, the PIV system allowed to couple the movement of grains with instantaneous point velocity measurements. Entrainment, displacement and deposition are accurately identified for more than 2 minutes per test and, hence, for increasing values of shear stress.

The 2009 database has been used with the aim to understand the deposition process. The visual inspection indeed brought to the idea of a possible grains clustering. To verify this thesis, a statistical analysis of particles location has been undertaken over time.

The Poisson test, able to state the random or not positions of grains, has to be considered highly consistent.

It is evident indeed that a significant number of cells of the investigated area are completely empty whilst some are abundant of particles.

The Chi Square coefficient's value was lower than the 5% value at the beginning, stating a random distribution, then it increased with time, showing that the stops position became less and less random with time and that the already deposited stops could strongly influence the new arriving particles.

The analogous trend of Moran and Gaery coefficients strengthened this theory.

The available PIV velocity data has allowed investigate a possible link between deposition and velocity, never studied so far.

Data has been double averaged, in time and space, to have a cells partition equals to the stops location one and to enable the calculation of a correlation coefficient.

For all the temporal window (the considered number of frames) and for all the tests, the correlation coefficient did not reach significant levels, with a maximum value of 0.19.

The flow filed is then not correlated to the deposition, the two physical magnitudes are independent and this suggests instead the likely significant role that bed roughness could have on the deposition process.

This deposition study, at this stage, showed some important aspect with respect to the grains motion mechanics, never investigated before.

For this reason it would be interesting to invest some time and efforts in other tests, able to describe deposition with the same accuracy that was developed for entrainment.

References

Anselin, L., *Moran's I as a regression coefficient*, 1980

Bottacin-Busolin, A., Tait, S.J., Marion, A., Chegini, A., Tregnaghi, M., 2008, *Probabilistic description of grain resistance from simultaneous flow field and grain motion measurements,* Water Resour. Res. , VOL 44

Drake, T.G., Shreve, R.L., Dietrichj, W.E., Whitings, P.J., Leopoldf, L.B., 1988, *Bedload transport of fine gravel observed by mo tion-pict ure photography,* J . Fluid Meeh. , vol. 192, p p . 193-217

Gomez, B., 1991, *Bedload transport*, Earth-Sei. Rec., 31: 89-132.

Grass, A.J., 1970, *Initial instability of fine bed sand*, Journal of the Hydraulics Division

Hassan, M.A., Church, M., 1994, *Vertical mixing of coarse particles in gravel bed rivers: A kinematic model,* Water Resour. Res. ,30 (4), 1173-1185

Nikora, V.I., Goring, D.G., Biggs, B.J.F., 1998, *On gravel-bed roughness characterization*, Water Resour. Res. ,34 (3), 517-527

Nikora, V.I., Habersack, H., Huber, T., McEwan, I., 2002, *On bed particle diffusion in gravel bed flows under weak bed load transport,* Water Resour. Res. ,38 (6)

Schmeeckle,M.W., Nelson, J.M., Shreve, R.L., 2007, *Forces on stationary particles in near-bed turbulent flows*, Journal of Geophysical Research, VOL 112

Tregnaghi, M., Bottacin-Busolin, A., Tait, S., Marion, A., 2012, *Stochastic determination of entrainment risk in uniformly sized sediment beds at low transport stages: 2. Experiments*, Journal Of Geophysical Research, Vol. 117, F04005

Van Rijn, L.C., 1984, *Sediment Transport, Part I: Bed Load Transport,* Journal Of Hydraulic Engineering, 110, 1431-1456

Wilcock, P.R., 1993, *Critical shear stress of natural sediments,* ASCE

Guarin, *Thesis*, 2010

http://www.lavision.de/en/techniques/piv.php

http://stattrek.com/chi-square-test/goodness-of-fit.aspx?Tutorial=AP

http://www.itl.nist.gov/div898/handbook/eda/section3/contour.htm